THE UNIVERSITY OF CHICAGO

MULTI-REFERENCED EXCITED STATES AND INTERMOLECULAR FORCES FROM THE ANTI-HERMITIAN CONTRACTED SCHRÖDINGER EQUATION

A DISSERTATION SUBMITTED TO
THE FACULTY OF THE DIVISION OF THE PHYSICAL SCIENCES
IN CANDIDACY FOR THE DEGREE OF
DOCTOR OF PHILOSOPHY

DEPARTMENT OF CHEMISTRY

BY

ERICA J. STURM

CHICAGO, ILLINOIS

AUGUST 2016

To GPL

For showing me that everything can teach me something.

TABLE OF CONTENTS

LIST OF FIGURES

LIST OF TABLES

ABSTRACT

Strong correlation due to multi-referenced electronic states of quantum chemical systems are crucial for a proper understanding of important phenomena including excited states, bond breakage and formation, singlet fission and biological transport. By solving for the 2-electron reduced density matrix (2-RDM) directly via the anti-Hermitian contracted Schrdinger equation (ACSE) we provide a balanced treatment of single and multi-referenced correlation effects without utilizing the N-electron wave function. This significantly reduces the computational expense while still maintaining near full configuration interaction accuracy when available. When provided with an initial 2-RDM guess from an active-space multi-configuration self consistent field wave function the ACSE scales as $r_a^2 r_e^4$ where r_a is the number of active molecular orbitals (MOs) and r_a is the number of external MOs.

This work demonstrates the energetic accuracy of ACSE calculations with several small multi-referenced systems and presents a novel approach for investigating intermolecular interactions, using a simple dimer test case. In this monomer-optimized basis set approach we compute each monomer's properties in isolation and obtain a set of natural orbitals that best describe the monomer. We then remove or truncate orbitals deemed excessive as a function of occupation number, defining a monomer molecular orbital basis uniquely suited to that monomer. Combining two such monomers yields a super-system expressed in the monomer basis which we then rotate to a dimer basis at a desired geometry before creating a new initial 2-RDM for the final optimization by an ACSE calculation. It is found that the intermolecular properties calculated in this fashion from larger atomic basis sets maintain their high accuracy but at a fraction of the computational cost. Furthermore this basis set optimization is free of basis set superposition error, circumventing the need for an expensive counterpoise correction.

ACKNOWLEDGMENTS

What a wonderfully strange journey graduate school has been. This has been the most challenging experience I have ever had, with so many unexpected twists and ultimately it has been worth the effort. It is odd and not a little surreal that after all this time it is now coming to a close. If someone had given me this document four years ago and said "You will defend this," I would not have believed it. I have learned so much during grad school, and not all of it is recorded here; so much more happened behind the scenes. But great things do not come from solo efforts, and this is no exception. I would like to take a moment before the main event and thank those who helped me along the way.

First, there is my family. They have been there since day one with everything from advice about choosing electives in high school to picking a college and finally my decision to come here. But they have also helped with smaller things like how to properly cook with a gas stove and telling me how to make radiators quiet down my first real winter up here. And of course, knowing that during breaks there was always a certain favorite movie to look forward to with Sharon and Harrison. My family's encouragement and belief that I could accomplish whatever I set out to do has been instrumental to my success throughout life.

The Mazziotti group has provided many learning opportunities for me and everyone here contributed something different to my education. I would like to thank Dr. David Mazziotti for accepting me in his group and providing the resources and guidance for the last few years. I would also like to acknowledge all of the group members, past and current that I have worked with: Greg, Jay, Srikant, Andrew, Erik, Chad, Nick, Valentine, Romit, Charles, Julie, Anthony, Manas, Ali, Kade, Claire, Alison and Lexie. Each person taught me something a little different, from new quantum chemistry theories to learning how to use the tools of the trade. Thank you all.

I would also like to acknowledge the friends outside of the lab that I made here too. It has been an absolute joy working with you and finding ways together to keep moving forward. To my first year office crew: Jeremy, Jacob, Valentine, Paul and Nolan, we absolutely had

the best office; I have many fond memories from the blur that was our first year. May you all have the highest quality nappin' chairs in your future workspaces! I also have good memories from time I spent with Hunter, Mary, Judith, and Seyit. Between concerts, board games, new restaurants and probably a metric ton of pizza there were many fun experiences I shared with all of these people. Their friendships helped shape my graduate career positively and I am grateful to them.

And there are the teachers that helped launch my education, providing me with the first stepping stones to get where I am today. I would like to thank Mrs. Teresita Chipi from Stoneman Douglas High School for demonstrating that magnesium combustion reaction so many years ago. That reaction still shines brightly as the day I knew I had to be a chemist. There are also Drs. Norito Takenaka and Rajeev Prabhakar and their groups at the University of Miami for providing me with my first research opportunities. Dr. Takenaka's lab taught me to think like a chemist and Dr. Prabhakar's group gave me my first introduction to computational chemistry, leading me to pursue my current research. Thank you for giving me opportunities, advice and guidance.

And lastly, I would like to thank Aaron for being the best result from a backfired experiment I could want. His support and level headed advice got me through several rough patches over the last two years. Even on the worst days he would be there to make it better and help me remember not take things too seriously. And he has been there to celebrate my successes with me, cheering me onwards. His many computer tricks that I now routinely use made my work less tedious and opened new doors to me. Being with him reminds me that excited states are not *just* for electrons in my code. Experiences together in and beyond Chicago have all been awesome because I got to share them with you.

CHAPTER 1

INTRODUCTION

Electronic structure is the study of electronic distribution and movement for a given state and nuclear geometry. While the Schrödinger equation provides a complete description of electronic behavior, we cannot solve it exactly for all systems and as a result we develop mathematical models to reproduce the physics of the system with varying degrees of accuracy. Generally when greater accuracy is desired, the models become more complex and thus more computationally expensive. These highly accurate models quickly become intractable as the number of electrons increases and the number of particle interactions grows factorially. Moreover, analytical solutions to these equations do not exist, only numerical resolutions. Our goal then as electronic structure scientists is to develop models and programs that accurately capture the physics of the quantum system while concurrently maintaining low computational expense.

1.1 The Hartree-Fock Approximation

A complete description of a chemical system's stationary states can be determined by solving the time-independent Schrödinger equation (TISE) for the N-electron wave function, Ψ [1]

$$\hat{\mathrm{H}}\Psi = E\Psi. \tag{1.1}$$

The simplest *ab initio* electronic structure approach for solving the Schrödinger equation and quite often the first step to subsequent calculations is the Hartree-Fock approximation [2]. This model provides a convenient framework for understanding how electrons occupy a system's orbitals such that the overall energy is minimized and therefore it is a good place to begin our discussion about electronic structure methods. At the outset we must assume that the total wave function, which describes all dynamics of the entire system, is separable into

nuclear and electronic components via the Born-Oppenheimer approximation [1, 3, 4]. Requiring the nuclei to be stationary with respect to electronic motion enables us to focus solely on the electronic problem. The electronic Hamiltonian that describes the orbital paths of N electrons in a field of M stationary nuclear point charges is given by the following expression:

$$\hat{\mathrm{H}} = \sum_{i=1}^{N} h_i + \sum_{i=1}^{N} \sum_{i \neq j}^{N} \frac{1}{r_{ij}}, \tag{1.2}$$

where the first summation represents the one-electron terms, comprised of the kinetic energy and the energy of the nuclear-electron interactions for each electron as shown below:

$$h_i = -\frac{1}{2}\nabla_i^2 - \sum_{J}^{M} \frac{Z_J}{r_{iJ}}. \tag{1.3}$$

The second addend in Eqn. 1.2 is the sum of the two-electron terms between all unique pairs of electrons. This contains the repulsive Coulumbic interaction energy between all electrons and the attractive exchange energy which only applies to pairs of electrons with parallel spin.

Variational optimization of Eqn. 1.2 yields a set of orbitals that minimizes the overall ground state system energy. By expressing these molecular orbitals as a linear combination of atomic orbitals in a finite atomic basis as Roothaan did, the eigenvalue equation in Eqn. 1.1 becomes a linear algebra matrix problem [2]. We now solve for the atomic orbital expansion coefficients that describe the molecular orbitals. This final Hartree-Fock wave function (Ψ_0) can be conveniently written as a Slater determinant:

$$\Psi_0(1, 2, \ldots, N) = (N!)^{-\frac{1}{2}} \begin{vmatrix} \theta_1(\mathbf{x}_1) & \theta_2(\mathbf{x}_1) & \cdots & \theta_N(\mathbf{x}_1) \\ \theta_1(\mathbf{x}_2) & \theta_2(\mathbf{x}_2) & \cdots & \theta_N(\mathbf{x}_2) \\ \vdots & \vdots & \ddots & \vdots \\ \theta_1(\mathbf{x}_N) & \theta_2(\mathbf{x}_N) & \cdots & \theta_N(\mathbf{x}_N) \end{vmatrix} \tag{1.4}$$

or more compactly:

$$\Psi_0(1, 2, \ldots, N) = |\theta_1(\mathbf{x}_1)\theta_2(\mathbf{x}_2)\ldots\theta_N(\mathbf{x}_N)\rangle\,, \tag{1.5}$$

$$= |\theta_1\theta_2\ldots\theta_N\rangle\,. \tag{1.6}$$

where the θ_N are the spin orbitals in columns and the $\mathbf{x}_N$ are electronic coordinates in rows. Using a Slater determinant also ensures that the fermionic wave function is anti-symmetric. That is, the interchange of any two electrons (rows) causes the overall wave function to change sign [5].

Remarkably, this straightforward method can capture ∼99% of the true ground state energy for a given basis involving first row elements [3, 5]. However, that last 1% is crucial for a complete system description as it often encodes chemically important behavior caused by instantaneous electron interactions. Hartree-Fock calculations cannot reproduce these interactions because each electron is treated separately and only experiences the remaining electrons as an *average* electrostatic field. Put another way, electronic motions are uncorrelated in the Hartree-Fock approximation.

1.2 The Electronic Correlation Problem

1.2.1 Strong Multi-Referenced Correlation

The mean-field Hartree-Fock approach cannot adequately model the wave function for systems with energetically degenerate or nearly degenerate molecular orbitals. If the lowest available orbitals are isoenergetic with at least one other, the Hartree-Fock approximation will be unable to place electrons in the lowest energy orbital because now several options exist. In that case the system is said to be strongly correlated [5–7]. Take for example the nitrogen molecule [8–10]. The molecular orbital diagram for N_2 near the equilibrium geometry region shows that the energy levels are well separated and it is clear which are lowest

Figure 1.1: The valence molecular orbital diagram of molecular nitrogen at three geometries. Diagram (a) shows N_2 at equilibrium where the molecular orbitals are clearly separated. Diagram (b) shows a stretched nuclear geometry and the molecular orbitals for the 2π bonds are becoming iso-energetic. Diagram (c) shows an even greater internuclear distances and now the 3σ molecular orbitals are also nearly iso-energetic with each other and the 2π orbitals.

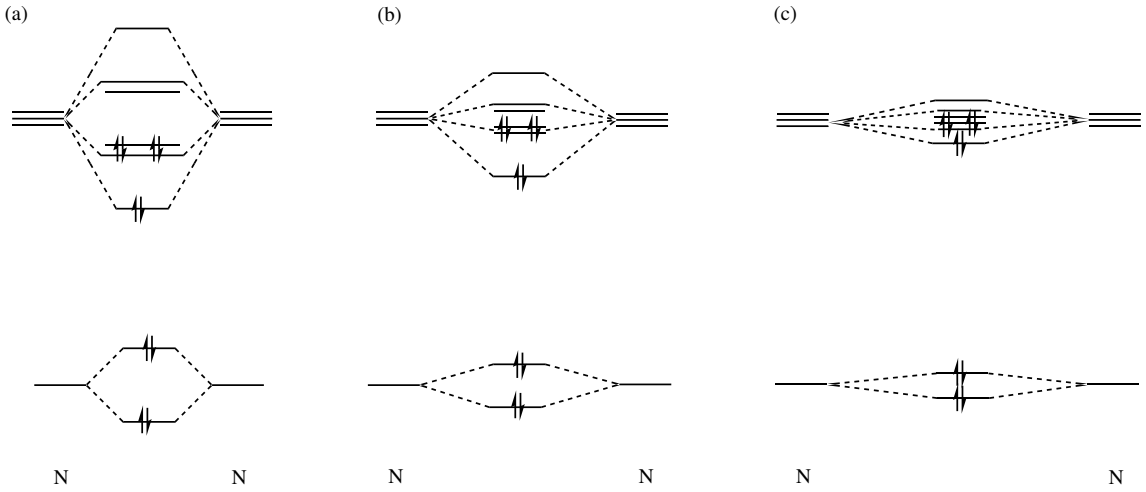

and therefore occupied. The equilibrium molecular orbital diagram is shown in image (a) of Fig. 1.1. But as the interatomic radius increases during dissociation the energy gap between the 2π and $2\pi^*$ orbitals decreases and approach degeneracy; multiple electronic configurations can now exist (image (b)). As the radius increases more the 3σ and $3\sigma^*$ energy gap also narrows and the number of degenerate orbitals becomes greater, further complicating the electronic configuration (image (c)). Ultimately the bonds break and the electrons on each atom interact with the other atom's electrons less and less. One single determinant cannot describe all possibilities described above and the Hartree-Fock approximation also breaks down.

In addition to dissociation curve degeneracies in the ground state, excited states are also frequently multi-referenced [11–13]. Using the N_2 ground state equilibrium molecular orbital diagram again, we can see that any of the four identical electrons in the 2π bonds can absorb an incoming photon of sufficient energy to induce an electronic transition in Fig. 1.2 (a). Once absorbed, there is further ambiguity as to which vacant $2\pi^*$ orbital would become

Figure 1.2: The molecular orbital diagram of a nitrogen molecule absorbing a photon. It is not clear which of the four electrons in the ground state 2π orbitals will absorb the incoming photon in diagram (a). Furthermore, there are two iso-energetic unoccupied $2\pi^*$ orbitals that can accept the excited electron in diagram (b).

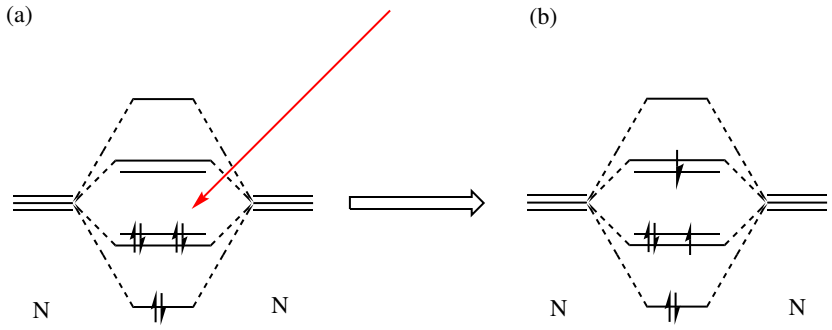

populated (b). This simple example has eight equally likely possibilities for the 2π electrons! This particular system and its dissociation as well as several of its excited states will be discussed in greater detail in Chapter 3.

Generally, ground states are easier to compute and have traditionally received more attention because they can be found variationally. If an excited state possess a different symmetry or multiplicity than the ground state, than a variational optimization may work in those cases as well. However, when a desired excited state shares these properties with any energetically lower state (including the ground state), a variational approach will not work directly. The excited state must be constrained to be orthogonal to those lower states [5, 12].

1.2.2 Correlation Energy Recovery: Full Configuration Interaction

Fortunately we can recover the missing energy caused by strong correlation effects by incorporating additional determinants into the wave function definition. Additional determinants can be generated via electronic excitation. Moving a single electron from its initial ground state orbital P to an unoccupied or virtual orbital, Q, defines a new excited state wave

function, Ψ_P^Q

$$\Psi_0 = |\chi_1(\mathbf{x}_1)\chi_2(\mathbf{x}_2)\dots\chi_P(\mathbf{x}_P)\dots\chi_N(\mathbf{x}_N)\rangle\,, \tag{1.7}$$

$$\Psi_P^Q = |\chi_1(\mathbf{x}_1)\chi_2(\mathbf{x}_2)\dots\chi_Q(\mathbf{x}_P)\dots\chi_N(\mathbf{x}_N)\rangle\,. \tag{1.8}$$

This is known as a single electronic excitation and can be done with any electron and any virtual orbital, provided that the electronic transition selection rules are obeyed [14]. Moving two ground state electrons to two virtual orbitals is a double excitation and this process can be extended to all electrons and orbitals within the system. By linearly combining all of the unique determinants for excited states we can derive a complete description of the wave function for a given basis comprised of every possible arrangement of electrons in orbitals [2] as defined in Eqn. 1.9 below:

$$\Psi = c_0\,|\psi_0\rangle + \sum_{ip} c_i^p\,|\psi_i^p\rangle + \sum_{i<j}\sum_{p<q} c_{ij}^{pq}\,|\psi_{ij}^{pq}\rangle + \sum_{i<j<k}\sum_{p<q<r} c_{ijk}^{pqr}\,|\psi_{ijk}^{pqr}\rangle + \dots \tag{1.9}$$

where $i, j, k, ...$ and $p, q, r, ...$ denote the ground state occupied and virtual orbitals respectively, and the $\{c\}$ are coefficients of the Slater determinants, $\{\psi\}$. ψ_0 is the initial ground state Hartree-Fock determinant. This expression of the wave function is known as the full configuration interaction (FCI) model and solving for it provides the best wave function description possible in a given finite basis.

The discrepancy between the true FCI energy and the Hartree-Fock energy is known as the correlation energy [2]

$$\mathrm{E_{corr}} = \varepsilon_{\mathrm{FCI}} - \mathrm{E_{HF}}. \tag{1.10}$$

By definition FCI expressions do not suffer from this computational artifact. Unfortunately, the FCI algorithm has factorial scaling with respect to the number of electrons and cannot be used for chemical systems with more than ∼16 electrons distributed amongst 16 spatial orbitals. As a result, FCI approximations can only be used for the smallest systems and with

minimal basis sets. The development of low cost polynomial scaling *ab initio* algorithms is thus of great importance for the study of electronic structure.

1.3 *Ab Initio* Wave Function Methods

Various *ab initio* methods have been developed to recover the correlation energy for lower computational cost. Since most of these methods (including FCI) rely on an initial Hartree-Fock wave equation they are considered post Hartree-Fock treatments of the wave function. Broadly, there are two main categories of these approaches: single and multi-referenced. Both can successfully reproduce the dynamic correlation that results from a single referenced system, but strong multi-referenced or static correlation presents a much greater challenge. In both categories at least one excited state is generated to improve the wave function expression, although how those excited states are produced varies.

Single referenced methods such as the coupled cluster hierarchy [15–17] generate a manifold of excited determinants using the initial Hartree-Fock approximation virtual orbitals. However, such approaches encounter difficulties because the mean-field solution poorly describes the unoccupied virtual orbitals that populate upon excitation. Other methods such as time-dependent density functional theory couple the ground state solution to a time dependent external potential field and measuring the response [11]. In contrast, multi-referenced techniques have the capability of describing degenerate or near degenerate molecular orbitals as described above, but they may also scale exponentially and occasionally require the selection of an active space [18, 19]. This selected subset of orbitals is treated with a higher level of theory and leaves any occupied orbitals outside of that active space uncorrelated.

The multi-configuration self-consistent field (MCSCF) family is perhaps the most widespread implementation of active space *ab initio* methods [2, 20]. With these models a subset of electrons and orbitals from an initial mean-field Hartree-Fock calculation are selected for treatment at a higher level of theory. This is known as the active space [5]. Inactive but occupied orbitals are called core orbital and the remaining unoccupied orbitals beyond the

active space are known as virtual orbitals. These latter two subsets of orbitals remain at the mean-field level of theory and receive no further treatment. However, the active space can be improved via several different algorithms [5]. The most common active space improvement is the complete active space self-consistent field (CASSCF) which is sometimes referred to as the full-optimized reaction space (FORS) [19]. This treatment is similar to a small-scale FCI calculation where every possible electronic configuration amongst all active space orbitals is computed and re-optimized as shown in Eqn. 1.9. As a result, the CASSCF approximation has the same computational limitations as a regular FCI calculation due to exponential scaling with respect to the number of active orbitals. Furthermore, despite their enormous flexibility, any active space routine, including CASSCF can be difficult to use since the selection of the active orbitals is usually accomplished manually and is more of a subjective art than a rigorous procedure.

Incorporating perturbation theory [21–24] can often lead to improved accuracy for both single and multi-referenced approaches, but improvements and even convergence are not necessarily guaranteed due to the lack of an iterative mechanism. Moreover this extra correction can only be applied successfully in cases where the system does not exhibit drastic changes, only small ones. Bond breakage, for example, is often too large a system alteration for perturbation theory. Generally, adding more approximations and steps increases the complexity of the solution and computational effort.

Further complicating the correlation recovery problem is that chemical behaviors rarely fit neatly into one type of correlation alone. Single-referenced methods work extremely well and outperform multi-referenced methods for many species in the ground state near their equilibrium geometries, but oftentimes we wish to examine systems not in their lowest electronic state or far removed from their equilibrium orientations. These regimes are of great importance chemically speaking because they provide insight into phenomena of interest such as transition states, charge transfer reactions and bond formation or breakage. Multi-reference methods typically have greater success in these situations. Ideally though we would

want one approach to accurately address both types of correlation.

1.4 Reduced Density Matrix Methods

1.4.1 Historical Background

Despite these advances in traditional wave function science, many of the issues associated with strong correlation calculations can be circumvented by utilizing a fundamentally different approach. Assuming that the electronic Hamiltonian describes the interactions of at most two indistinguishable particles, the N-electron wave function contains significantly more information than is required for quantum property calculations. Coleman realized this and posited in 1951 that the N-electron problem could be reduced to a two particle problem [25]. To that end Mayer attempted to variationally determine the ground state energy of a system with the 2-electron reduced density matrix (2-RDM) instead of the wave function in 1955 [26]. However, he found that the computed energy was *lower* than the true answer! Soon afterwards Coleman and several others determined that additional constraints on the 2-RDM were required to ensure that it came from the desired N-electron wave function. The search for these necessary and sufficient conditions became known as the *N-representability problem* [27]. Despite these unknown constraints, RDMs remained an intriguing approach to solving many-electron system questions.

For several decades RDM science grew slowly; new RDMs expressions were developed but little progress was made regarding the N-representability conditions [28], preventing useful applications of RDM techniques. Then, in the early 1990s Valdemoro demonstrated [29, 30] how the higher order RDMs could be reconstructed from the lower ones. This paved the way for the development of an iterative solution to the contracted Schrödinger equation (CSE) [31]. Since then several more algorithms for the computation of the 2-RDM have emerged, broadly sorted into two categories: the variational minimization of the ground state energy expressed as a functional of the 2-RDM and the iterative solution of the CSE

and its Hermitian and anti-Hermitian components.

1.4.2 The Variational Approach for Obtaining 2-RDMs

In the first category, one can variationally minimize the ground state energy of the 2-RDM by applying known N-representability constraints [32]. Namely, the positivity conditions must be met. The ^{2}D positive semi-definite condition is the requirement that the eigenvalues of the 2-RDM ($^2\mathbf{D}$) are strictly non-negative [33]. Physically this means that the probability of finding two electrons in two orbitals is always greater than or equal to 0. Similarly the ^{2}Q condition ensures the probability of *not* finding two electrons (i.e. holes) in two orbitals is also greater than or equal to zero. The ^{2}G condition requires that the probability of finding one electron in an orbital and a hole in another orbital is non-negative as well. Collectively, these constraints on the 2-RDM are called the 2-positivity conditions. Analogously, there are the 1-positivity conditions where the ^{1}D and ^{1}Q conditions for the 1-RDM ($^1\mathbf{D}$) are similar to the ^{2}D and ^{2}Q conditions respectively. In 2001 Mazziotti and Erdahl [34] showed how the positivity conditions for generic higher order RDMs could be determined. Soon afterwards the first trials implementing some of them were performed using semi-definite programming techniques [35] as a means of enforcing these constraints [36, 37]. These positivity requirements on the solution to the variational approach are strong enough to provide reliable, physical results.

Another way to ensure that the known N-represntability conditions are met is to parametrize the wave function and thus the subsequent 2-RDM upon integration. Initially pioneered by Kollmar in 2006 [38], this method was developed as means to make a configuration interaction approximation with doubles (CID) size consistent. That is, that the energy of two isolated systems is equal to that where the same two particles are infinitely separated in a single system. This was accomplished by the incorporation of a topological factor for the expansion coefficients of the CID wave function that relied on the Cauchy-Schwarz inequalities of the 2-positivity conditions described above, but may not actually satisfy those same

conditions. In the following years DePrince and Mazziotti [39] and Mazziotti [40] further modified the method by explicitly including single excitations (i.e. CISD) and modifying the topological factor to satisfy the 2-positivity conditions described above. This procedure is known as the parametric variational method.

1.4.3 Contracted Schrödinger Equation Methods for Obtaining 2-RDMs

The second category of methods used to compute the 2-RDM is accomplished by iteratively solving a contracted form of the Schrödinger equation rather than the normal Schrödinger equation for the N-electron wave function, Ψ_N [25, 41, 42]. The remainder of this work will utilize a specific form of the contracted Schrödinger equation (CSE) for computing ${}^2\mathbf{D}$, and so we now take the time to explicitly introduce terminology and some notation.

As previously stated, the energy of a quantum system can be expressed as a linear functional of the 2-RDM without relying upon the N-electron wave function:

$$E = \mathrm{Tr}({}^2\mathbf{K}\ {}^2\mathbf{D}) \tag{1.11}$$

$$= \sum\ {}^2K^{i,j}_{k,l}\ {}^2D^{i,j}_{k,l}. \tag{1.12}$$

In the above equations the original Hamiltonian from the Schrödinger equation has been mapped to its 2-particle reduced Hamiltonian counterpart ${}^2\mathbf{K}$ defined as

$${}^2\hat{\mathrm{K}} = N\Big(\frac{\nabla^2}{2} - \sum_J^M \frac{Z_J}{r_{1J}}\Big) + \frac{N(N-1)}{2}\frac{1}{r_{12}}, \tag{1.13}$$

where N is the total number of electrons and M is the total number of nuclei. To use Eqn. 1.11 to obtain the energy of a system we also need a 2-RDM. We will be using the anti-Hermitian part of the CSE in a method called the anti-Hermitian contracted Schrödinger equation (ACSE) and briefly describe how it is derived from the CSE below.

To derive the CSE and subsequently the ACSE we begin with the (TISE) written in

density matrix form [43–45].

$$\hat{\mathrm{H}}^N D_n = \mathrm{E_n}\,{}^N D_n \tag{1.14}$$

where ${}^N D_n = \Psi_n \Psi_n^*$ is the N-particle density matrix in its n^{th} state. The Hamiltonian is Hermitian so the equation can be decomposed into a pair of separate equations, one of which will be Hermitian and the other anti-Hermitian.

$$\frac{1}{2}(\hat{\mathrm{H}}^N D_n +^N D_n \hat{\mathrm{H}}) = \mathrm{E_n}\,{}^N D_n, \tag{1.15}$$

$$\frac{1}{2}(\hat{\mathrm{H}}^N D_n -^N D_n \hat{\mathrm{H}}) = 0. \tag{1.16}$$

Visual inspection confirms that the sum of these two equations is identical to the original Schrödinger equation . By definition the Hermitian portion of the decomposition (Eqn. 1.15) must greater than or equal to zero and the anti-Hermitian equation (Eqn. 1.16) must be strictly imaginary or zero, not complex. Because the original right hand side of the Schrödinger equation is real and positive, it is associated with the Hermitian equation and the anti-Hermitian equation is identically equal to zero.

Integration (contraction) over spin and spatial coordinate of all save two of the electrons in each case leads to the contracted Schrödinger equation (CSE), the Hermitian contracted Schrödinger equation (HCSE), and the anti-Hermitian contracted Schrödinger equation (ACSE) as well as the 2 electron reduced density matrix (2-RDM), ${}^2 D_n$ [42, 44].

$$\int (\hat{\mathrm{H}}^N D_n)\mathrm{d3}\cdots\mathrm{dN} = \mathrm{E_n}\,{}^2 D_n, \tag{1.17}$$

$$\frac{1}{2}\int (\hat{\mathrm{H}}^N D_n +^N D_n \hat{\mathrm{H}})\mathrm{d3}\cdots\mathrm{dN} = \mathrm{E_n}\,{}^2 D_n, \tag{1.18}$$

$$\frac{1}{2}\int (\hat{\mathrm{H}}^N D_n -^N D_n \hat{\mathrm{H}})\mathrm{d3}\cdots\mathrm{dN} = 0. \tag{1.19}$$

With the appropriate N-representability constraints on the 2-RDM, the CSE, HCSE and ACSE can be all be solved for a desired ground or excited state. Without these conditions

it is possible that a 2-RDM solution to the CSE would not be N-representable and provide non-physical energetic predictions [27]. The 2-RDM provided by any of these approaches can be used in Eqn. 1.11 to obtain a final energy for the system.

Greater detail about the CSE and its Hermitian and anti-Hermitian counterparts will be provided in Chapter 2 with emphasis on the ACSE algorithm. Chapter 3 compares the performance of ACSE routine against other more traditional wave function methods with several small molecules. Chapter 4 presents current research and background regarding intermolecular interactions and relevant electronic structure challenges in that field. Finally, Chapter 5 presents a novel approach to addressing those intermolecular interactions as well as preliminary data, discussion, and conclusions.

1.5 References

[1] D. J. Griffiths, *Introduction to Quantum Mechanics*. Upper Sadle River, NJ: Prentice Hall, Inc., 1 ed., 1995.

[2] N. S. Szabo, Attila; Ostlund, *Modern Quantum Chemistry: Introduction to Advanced Electronic Structure Theory*. Mineola, New York: Dover Publications, Inc., 1 ed., 1982.

[3] T. Helgaker, P. Jørgensen, and J. Olsen, *Molecular Electronic-Structure Theory*. West Sussex, England: John Wiley & Songs Ltd., 1 ed., 2000.

[4] L. S. Cederbaum, "The exact molecular wavefunction as a product of an electronic and a nuclear wavefunction," *J. Chem. Phys.*, vol. 138, p. 224110, jun 2013.

[5] F. Jensen, *Introduction to Computational Chemistry, 2nd Edition*. West Sussex, England: Wiley, 2nd ed., 2007.

[6] V. Anisimov and Y. Izyumov, *Electronic Structure of Strongly Correlated Materials*, vol. 163 of *Springer Series in Solid-State Sciences*. Berlin, Heidelberg: Springer Berlin Heidelberg, 2010.

[7] D. W. Small and M. Head-Gordon, "Post-modern valence bond theory for strongly correlated electron spins.," *Phys. Chem. Chem. Phys.*, vol. 13, pp. 19285–97, nov 2011.

[8] A. Engels-Putzka and M. Hanrath, "Dissociating N 2 : a multi-reference coupled cluster study on the potential energy surfaces of ground and excited states," *Mol. Phys.*, vol. 107, pp. 143–155, jan 2009.

[9] W. C. Ermler, A. D. McLean, and R. S. Mulliken, "Ab initio study of valence-state potential energy curves of nitrogen," *J. Phys. Chem.*, vol. 86, pp. 1305–1314, apr 1982.

[10] H. Larsen, J. Olsen, P. Jørgensen, and O. Christiansen, "Full configuration interaction benchmarking of coupled-cluster models for the lowest singlet energy surfaces of N[sub 2]," *J. Chem. Phys.*, vol. 113, p. 6677, oct 2000.

[11] A. Dreuw and M. Head-Gordon, "Single-reference ab initio methods for the calculation of excited states of large molecules.," *Chem. Rev.*, vol. 105, pp. 4009–37, nov 2005.

[12] J. B. Foresman, M. Head-Gordon, J. A. Pople, and M. J. Frisch, "Toward a systematic molecular orbital theory for excited states," *J. Phys. Chem.*, vol. 96, pp. 135–149, jan 1992.

[13] L. González, D. Escudero, and L. Serrano-Andrés, "Progress and challenges in the calculation of electronic excited states.," *Chemphyschem*, vol. 13, pp. 28–51, jan 2012.

[14] D. A. McQuarrie, *Quantum Chemistry*. Susalito, California: University Science Books, second ed., 2008.

[15] A. I. Krylov, "Equation-of-motion coupled-cluster methods for open-shell and electronically excited species: the Hitchhiker's guide to Fock space.," *Annu. Rev. Phys. Chem.*, vol. 59, pp. 433–62, jan 2008.

[16] R. J. Bartlett, "Coupled-cluster theory and its equation-of-motion extensions," *Wiley Interdiscip. Rev. Comput. Mol. Sci.*, vol. 2, pp. 126–138, jan 2012.

[17] M. Musiał, S. A. Kucharski, and R. J. Bartlett, "Equation-of-motion coupled cluster method with full inclusion of the connected triple excitations for ionized states: IP-EOM-CCSDT," *J. Chem. Phys.*, vol. 118, p. 1128, jan 2003.

[18] R. Diffenderfer and D. Yarkony, "Use of the state-averaged MCSCF procedure: application to radiative transitions in magnesium oxide," *J. Phys. Chem.*, vol. 86, no. 26, pp. 5098–5105, 1982.

[19] M. W. Schmidt and M. S. Gordon, "The construction and interpretation of MCSCF wavefunctions.," *Annu. Rev. Phys. Chem.*, vol. 49, pp. 233–66, jan 1998.

[20] A. C. Wahl and G. Das, "The Multiconfiguration Self-Consistent Field Method," in *Methods Electron. Struct. Theory*, pp. 51–78, Boston, MA: Springer US, 1977.

[21] K. Andersson, P.-Å. Malmqvist, B. O. Roos, A. J. Sadlej, and K. Wolinski, "Second-order perturbation theory with a CASSCF reference function," *J. Phys. Chem.*, vol. 94, pp. 5483–5488, jul 1990.

[22] R. J. Bartlett, "Many-Body Perturbation Theory and Coupled Cluster Theory for Electron Correlation in Molecules," *Annu. Rev. Phys. Chem.*, vol. 32, pp. 359–401, oct 1981.

[23] J. Finley and P.-Å. Malmqvist, "The multi-state CASPT2 method," *Chem. Phys. ...*, vol. 288, no. 2, pp. 299–306, 1998.

[24] K. Hirao, "Multireference MøllerPlesset method," *Chem. Phys. Lett.*, vol. 190, pp. 374–380, mar 1992.

[25] C. A. Coleman and V. I. Yukalov, *Reduced Density Matrices: Coulson's Challenge*. Springer, 2000.

[26] J. Mayer, "Electron Correlation," *Phys. Rev.*, vol. 100, pp. 1579–1586, dec 1955.

[27] A. Coleman, "The structure of fermion density matrices," *Rev. Mod. Phys.*, vol. 175, no. 35, pp. 668–687, 1962.

[28] R. M. Erdahl, "Representability," *Int. J. Quantum Chem.*, vol. 13, pp. 697–718, jun 1978.

[29] C. Valdemoro, "Approximating the second-order reduced density matrix in terms of the first-order one," *Phys. Rev. A*, vol. 45, pp. 4462–4467, apr 1992.

[30] F. Colmenero and C. Valdemoro, "Approximating q -order reduced density matrices in terms of the lower-order ones. II. Applications," *Phys. Rev. A*, vol. 47, pp. 979–985, feb 1993.

[31] F. Colmenero and C. Valdemoro, "Self-consistent approximate solution of the second-order contracted Schrodinger equation," *Int. J. Quantum Chem.*, vol. 51, pp. 369–388, sep 1994.

[32] D. A. Mazziotti, "Quantum chemistry without wave functions: two-electron reduced density matrices.," *Acc. Chem. Res.*, vol. 39, pp. 207–15, mar 2006.

[33] D. A. Mazziotti, "Variational minimization of atomic and molecular ground-state energies via the two-particle reduced density matrix," *Phys. Rev. A*, vol. 65, p. 062511, jun 2002.

[34] D. A. Mazziotti and R. M. Erdahl, "Uncertainty relations and reduced density matrices: Mapping many-body quantum mechanics onto four particles," *Phys. Rev. A - At. Mol. Opt. Phys.*, vol. 63, pp. 1–9, mar 2001.

[35] D. A. Mazziotti, "Realization of quantum chemistry without wave functions through first-order semidefinite programming.," *Phys. Rev. Lett.*, vol. 93, p. 213001, nov 2004.

[36] T. Juhasz, N. Shenvi, and D. A. Mazziotti, "Recursively generated linear constraints

for variational two-particle reduced-density-matrix theory," *Chem. Phys. Lett.*, vol. 445, no. 4-6, pp. 79–83, 2007.

[37] G. Gidofalvi and D. A. Mazziotti, "Molecular properties from variational reduced-density-matrix theory with three-particle N-representability conditions.," *J. Chem. Phys.*, vol. 126, p. 024105, jan 2007.

[38] C. Kollmar, "A size extensive energy functional derived from a double configuration interaction approach: The role of N representability conditions," *J. Chem. Phys.*, vol. 125, no. 8, p. 084108, 2006.

[39] A. E. DePrince and D. A. Mazziotti, "Parametric approach to variational two-electron reduced-density-matrix theory," *Phys. Rev. A*, vol. 76, p. 042501, oct 2007.

[40] D. A. Mazziotti, "Parametrization of the two-electron reduced density matrix for its direct calculation without the many-electron wave function: Generalizations and applications," *Phys. Rev. A*, vol. 81, p. 062515, jun 2010.

[41] D. A. Mazziotti, "Two-electron reduced density matrix as the basic variable in many-electron quantum chemistry and physics.," *Chem. Rev.*, vol. 112, pp. 244–62, jan 2012.

[42] C. Valdemoro and D. R. Alcoba, *Frontiers in Quantum Systems in Chemistry and Physics*, vol. 18 of *Progress in Theoretical Chemistry and Physics*. Dordrecht: Springer Netherlands, 2008.

[43] R. McWeeny, "Some recent advances in density matrix theory," *Rev. Mod. Phys.*, vol. 32, pp. 335–369, apr 1960.

[44] G. Gidofalvi and D. A. Mazziotti, "Direct calculation of excited-state electronic energies and two-electron reduced density matrices from the anti-Hermitian contracted Schrödinger equation," *Phys. Rev. A*, vol. 80, p. 022507, aug 2009.

[45] E. J. Sturm and D. A. Mazziotti, "Highly accurate excited-state energies from direct computation of the 2-electron reduced density matrix by the anti-Hermitian contracted Schrödinger equation," *Mol. Phys.*, vol. 114, pp. 335–343, sep 2015.

CHAPTER 2

THE ANTI-HERMITIAN CONTRACTED SCHRÖDINGER EQUATION

There are two ways to directly compute the 2-electron reduced density matrix (2-RDM). The first consists of a variational minimization [1–3] with respect to the 2-RDM which is constrained by the N-representability conditions [4, 5]. The second iteratively solves for the 2-RDM solution of the contracted Schrödinger equation (CSE) [6–8]. In this chapter we will discuss a specific instantiation of the latter technique, known as the anti-Hermitian contracted Schrödinger equation (ACSE) [1, 9].

2.1 Derivation of the Contracted Schrödinger Equation

In Chapter 1 we described the derivation of the Contracted Schrödinger Equation (CSE) using a density matrix approach. Alternatively we can derive the same equations using the more compact notation of second quantization as shown here. Contraction or integration of the Schrödinger equation onto a two particle space immediately yields the CSE [13, 14]:

$$\langle\Psi|\hat{a}_i^\dagger\hat{a}_j^\dagger\hat{a}_k\hat{a}_l\hat{H}|\Psi\rangle = E\ {}^2D_{l,k}^{i,j} \tag{2.1}$$

where the annihilation operator $\hat{a}_p$ destroys an electron in spin orbital p and the adjoint creation operator $\hat{a}_q^\dagger$ creates an electron in spin orbital q. We now define a 2-electron reduced density operator (2-RDO) [14] such that its expectation value is the 2-RDM.

$${}^2\hat{\Gamma}_{l,k}^{i,j} = \hat{a}_i^\dagger\hat{a}_j^\dagger\hat{a}_k\hat{a}_l, \tag{2.2}$$

$${}^2D_{l,k}^{i,j} = \langle\Psi|\hat{\Gamma}_{l,k}^{i,j}|\Psi\rangle\,. \tag{2.3}$$

The CSE can now be rewritten as follows:

$$\langle\Psi|\hat{\Gamma}^{i,j}_{l,k}\ \hat{H}|\Psi\rangle\ =\ E\ {}^2D^{i,j}_{l,k}. \tag{2.4}$$

As before, the operator on the left hand side is Hermitian and thus the CSE may be re-expressed as two separate equations, one Hermitian and one anti-Hermitian.

$$\langle\Psi|\{\hat{\Gamma}^{i,j}_{l,k}, \hat{H}\}|\Psi\rangle = 2E\ {}^2D^{i,j}_{l,k} \tag{2.5}$$

$$\langle\Psi|[\hat{\Gamma}^{i,j}_{l,k}, \hat{H}]|\Psi\rangle = 0 \tag{2.6}$$

where the braces ({ }) indicate the anti-commutator and the brackets ([ ]) indicate the commutator [15].

The N-electron Hamiltonian operator can also be rewritten in a 2-particle reduced form:

$$\begin{aligned}\hat{\mathrm{H}} &= \frac{1}{2}\sum_{i,j;k,l}\ {}^2K^{i,j}_{l,k}\ \hat{a}^\dagger_i\hat{a}^\dagger_j\hat{a}_k\hat{a}_l \\ &= \sum_{i,k}\ {}^1K^i_k\ \hat{a}^\dagger_i\hat{a}_k\ +\ \sum_{i,j,k,l}\ {}^2V^{i,j}_{l,k}\hat{a}^\dagger_i\hat{a}^\dagger_j\hat{a}_k\hat{a}_l\end{aligned} \tag{2.7}$$

where ${}^2K$ is the 2 particle reduced Hamiltonian and ${}^1K$ and ${}^2V$ are the one and two electron integral terms respectively [9]. Combining Eqns. 2.4 and 2.7 enables us to express the system energy as a linear functional of the 2-RDM as shown in Chapter 1

$$E = \mathrm{Tr}\big({}^2\mathbf{K}\ {}^2\mathbf{D}\big). \tag{2.8}$$

2.2 The Necessity of Higher Order RDMs

2.2.1 Second Quantization Rearrangement

Rearrangement of the creation and annihilation operators in the second quantized form of the the HCSE and the ACSE indicate that higher order RDMs are required to solve for the 2-RDM [14, 16]. This can be demonstrated by utilizing the 2 particle reduced Hamiltonian (Eqn. 2.7) in conjunction with the CSE defined with RDM notation (Eqn. 2.4):

$$\begin{aligned} 2E^2 D^{i,j}_{l,k} &= \langle\Psi|^2\hat{\Gamma}^{i,j}_{l,k}\ {}^2\hat{H}|\Psi\rangle \\ &= \langle\Psi|\Big(\hat{a}^\dagger_i\hat{a}^\dagger_j\hat{a}_k\hat{a}_l\Big)\Big(\sum_{p,q}\ {}^1K^p_q\ \hat{a}^\dagger_p\hat{a}_q\ +\sum_{p,q;s,r}\ {}^2V^{p,q}_{s,r}\ \hat{a}^\dagger_p\hat{a}^\dagger_q\hat{a}_r\hat{a}_s\Big)|\Psi\rangle\,. \end{aligned} \tag{2.9}$$

By using the anti-commutation rule with δ^m_n as the Kronecker delta

$$\{\hat{a}^\dagger_m,\hat{a}_n\}\ =\ \hat{a}^\dagger_m\hat{a}_n+\hat{a}_n\hat{a}^\dagger_m\ =\ \delta^m_n, \tag{2.10}$$

the operators in Eqn. 2.9 can be rearranged such that all of the creation operators precede the annihilation operators in each term [17]:

$$\begin{aligned} E\ {}^2D^{i,j}_{k,l} = &\sum_s\Big({}^1K^k_s\ {}^2D^{i,j}_{l,s}-\ {}^1K^l_s\ {}^2D^{i,j}_{k,s}\Big)+3\sum_{p,s}\ {}^1K^p_s\ {}^3D^{i,j,p}_{s,k,l}+2\sum_{s,t}\ {}^2V^{k,l}_{s,t}\ {}^2D^{i,j}_{s,t} \\ &+6\sum_{q,s,t}\Big({}^2V^{l,q}_{s,t}\ {}^3D^{i,j,q}_{s,t,k}-\ {}^2V^{k,q}_{s,t}\ {}^3D^{i,j,q}_{s,t,l}\Big)+12\sum_{p,q,s,t}\ {}^2V^{p,q}_{s,t}\ {}^4D^{i,j,p,q}_{s,t,k,l}. \end{aligned} \tag{2.11}$$

This procedure reveals the necessity of two previously undefined p-RDMs in solving the CSE, namely the 3- and the 4-RDM [9, 15, 16] as shown below:

$${}^3D^{a,b,c}_{z,y,x} = \langle\Psi|\hat{a}^\dagger_a\hat{a}^\dagger_b\hat{a}^\dagger_c\hat{a}_x\hat{a}_y\hat{a}_z|\Psi\rangle\,, \tag{2.12}$$

$${}^4D^{a,b,c,d}_{z,y,x,w} = \langle\Psi|\hat{a}^\dagger_a\hat{a}^\dagger_b\hat{a}^\dagger_c\hat{a}^\dagger_d\hat{a}_w\hat{a}_x\hat{a}_y\hat{a}_z|\Psi\rangle\,. \tag{2.13}$$

The CSE in Eqn. 2.11 can also be split into a pair of Hermitian and an anti-Hermitian equations to obtain the HCSE and the ACSE. Doing so reveals that while the HCSE also relies directly upon both the 3- and 4-RDM the ACSE only requires the 3-RDM [9]:

$$\begin{aligned} 0 = &\sum_{s} \left({}^{1}K^{k}_{s}\ {}^{2}D^{i,j}_{s,l} - {}^{1}K^{l}_{s}\ {}^{2}D^{i,j}_{s,k} \right) + \sum_{p} \left({}^{1}K^{p}_{j}\ {}^{2}D^{p,i}_{k,l} - {}^{1}K^{p}_{i}\ {}^{2}D^{p,j}_{k,l} \right) \\ &+ 6 \sum_{p,s,t} \left({}^{2}V^{p,k}_{s,t}\ {}^{3}D^{i,j,p}_{s,t,l} - {}^{2}V^{p,l}_{s,t}\ {}^{3}D^{i,j,p}_{s,t,k} \right) + 6 \sum_{p,q,s} \left({}^{2}V^{p,q}_{s,j}\ {}^{3}D^{q,q,i}_{k,l,s} - {}^{2}V^{p,q}_{s,i}\ {}^{3}D^{p,q,j}_{k,l,s} \right) \\ &+ 2 \sum_{s,t} {}^{2}V^{k,l}_{s,t}\ {}^{2}D^{i,j}_{s,t} + 2 \sum_{p,q} {}^{2}V^{p,q}_{j,i}\ {}^{2}D^{p,q}_{k,l}. \end{aligned} \tag{2.14}$$

The computational expense of generating the higher order 3- and 4-RDMs from an initial wave function would be far too excessive to be of merit. This issue is circumvented by reconstructing them as functionals of lower order 1- and 2-RDMs via cumulant expansion.

2.2.2 Cumulant Expansion

We start with the definition of a Grassman algebra operator known as the anti-symmetric tensor product, more colloquially known as a wedge product. Wedging two functions together is defined as adding up all terms after anti-symmetric permutations of superscripts and subscripts and dividing the end result by the total number of unique terms. For example, the 2-RDM can be expressed as the wedge product of the 1-RDM with itself:

$$\begin{aligned} {}^{2}D^{i,j}_{l,k} &= {}^{1}D^{i}_{l} \wedge {}^{1}D^{j}_{k} + {}^{2}\Delta \\ &= \frac{1}{2}({}^{1}D^{i}_{l}\ {}^{1}D^{j}_{k} - {}^{1}D^{i}_{k}\ {}^{1}D^{j}_{l}) + {}^{2}\Delta. \end{aligned} \tag{2.15}$$

This mathematical definition allows us to express higher order RDMs with the following hierarchy where orbital indexes (superscripts and subscripts) have been suppressed for clarity:

$$^1D = {}^1\Delta, \tag{2.16}$$

$$^2D = {}^1D \wedge {}^1D + {}^2\Delta, \tag{2.17}$$

$$^3D = {}^1D \wedge {}^1D \wedge {}^1D + 3\,{}^2\Delta \wedge {}^1D + {}^3\Delta. \tag{2.18}$$

The ${}^n\Delta$ terms are known as cumulant n-RDMs and they represent the connected part of the RDMs. Their presence (absence) denotes statistical dependence (independence) of the relevant particles [15]. The cumulant 2-RDM ${}^2\Delta$ can be determined via ${}^2\Delta = {}^2D - {}^1D \wedge {}^1D$, but the reconstruction of ${}^3D$ with the cumulant 3-RDM, ${}^3\Delta$, is not as straightforward. Over the years several approximations with various accuracies have been made [18–20]. In this work we make use of the Mazziotti reconstruction scheme [8, 21, 22] of the 3-RDM where the cumulant 3-RDM ${}^3\Delta$ is approximated as

$$n^{i,j,k}_{q,s,t}\,{}^3\Delta^{i,j,k}_{q,s,t} \approx -\frac{1}{6}\sum_l \hat{A}({}^2\Delta^{i,l}_{q,s}\,{}^2\Delta^{j,k}_{l,t}) \tag{2.19}$$

where $\hat{A}$ is the anti-symmetrizing operator and

$$n^{i,j,k}_{q,s,t} = {}^1D^i_i + {}^1D^j_j + {}^1D^k_k + {}^1D^q_q + {}^1D^t_t + {}^1D^s_s - 3. \tag{2.20}$$

This particular reconstruction for the cumulant 3-RDM is second order. With a concise algorithm for the generation of the higher order 3-RDM as a functional of the lower order 1- and 2-RDMs, we are now ready to solve the ACSE for an optimized 2-RDM.

2.3 Solving The ACSE

Solving the ACSE for an N-representable 2-RDM begins with an initial wave function guess, $\Psi(0)$. This guess may be either the result of a single-referenced approach such as a Hartree-Fock approximated wave function [15], or a multi-referenced approach such as complete active space self consistent field (CASSCF) [14]. Details about the Hartree-Fock and CASSCF algorithms can be found in Chapter 1. It is important to note that a 'solution' to the ACSE indicates that the resultant 2-RDM's electronic energy has been minimized, but that minimal error may still exist. Ultimately the ACSE is solved by an infinite series of ordered unitary transformations, but in practice there are two stopping criterion which will be described later in this section. The expression of Ψ as a function of the variable λ is used to order these unitary transformations and in that regard, λ is a time-like parameter. It exists solely as an organization metric.

To take an infinitely small step forward in λ by an interval ϵ, the associated unitary rotation matrix is given by an exponential of an anti-Hermitian operator, $e^{\epsilon S(\lambda)}$, which is simplified via power series expansion [15]. The energy at $\lambda + \epsilon$ is given by

$$\begin{aligned} E(\lambda+\epsilon) &= \langle\Psi(\lambda)|e^{-\epsilon S(\lambda)}\hat{H}e^{\epsilon S(\lambda)}|\Psi(\lambda)\rangle \\ &= E(\lambda) + \epsilon\ \langle\Psi(\lambda)|\big[\hat{H},\hat{S}(\lambda)\big]|\Psi(\lambda)\rangle + \mathcal{O}(\epsilon^2). \end{aligned} \tag{2.21}$$

Truncation of the power series expansion in Eqn. 2.21 at the second order (i.e. ϵ^2) and taking the limit of $\epsilon \to 0$ provides a differential equation that explains how the energy changes with respect to the ordering variable λ:

$$\frac{dE}{d\lambda} = \langle\Psi(\lambda)|\big[\hat{H},\hat{S}(\lambda)\big]|\Psi(\lambda)\rangle\,. \tag{2.22}$$

Using the same procedure we can derive an analogous expression for the 2-RDM itself as a

function of λ. Instead of the Hamiltonian operator, the 2-RDO is used in this case [11, 15]:

$$\frac{d^2 D^{i,j}_{l,k}}{d\lambda} = \langle \Psi(\lambda) | \left[{}^2\hat{\Gamma}^{i,j}_{l,k}, \hat{S}(\lambda) \right] | \Psi(\lambda) \rangle \,. \tag{2.23}$$

Restricting the anti-Hermitian operator $\hat{S}$ in Eqn. 2.21 to possess no more than two body interaction terms permits us to express the variational degrees of freedom for the operator as a 2-particle reduced matrix whose elements are given by

$${}^2\hat{S}(\lambda) = \sum_{i,j,k,l} {}^2S^{i,j}_{l,k} \hat{a}^\dagger_i \hat{a}^\dagger_j \hat{a}_k \hat{a}_l. \tag{2.24}$$

At each step of ϵ in the λ parameter, the energy of the system is minimized with respect to these $\hat{S}$ matrix elements. That is,

$$\begin{aligned} {}^2\hat{S}^{i,j}_{l,k}(\lambda) &= -\frac{1}{\epsilon} \frac{\partial E(\lambda + \epsilon)}{\partial({}^2S^{i,j}_{l,k}(\lambda))} \Big|_{{}^2S=0} \\ &= \langle \Psi(\lambda) | \left[{}^2\Gamma^{i,j}_{l,k}, \hat{H} \right] | \Psi(\lambda) \rangle \,. \end{aligned} \tag{2.25}$$

These sets of differential equations expressed as in the $\hat{S}$ matrix form can be solved to produce a new 2-RDM that satisfies the ACSE. At each step in λ, a new 2-RDM is produced and is compared to the previous step's result [15]. This process is propagated along λ until a stop condition is achieved. A final solution is attained when either (i) the least-squares error of the ACSE increases or (ii) the computed energy from a 2-RDM increase s [14]. The former is more common. The ACSE has a computational scaling equal to r^6 where r is the total number of spatial orbitals or rank of the chosen basis set [9, 15] when a single-referenced wave function is provided as the initial 2-RDM. When an active space method such as CASSCF (see Chapter 1) produces the initial 2-RDM for the ACSE algorithm the ACSE scales as $r_a^2 r_e^4$ where r_a and r_e are the number of active and virtual orbitals respectively [11].

2.4 Advantages of the ACSE

2.4.1 Comparison to Wave Function Methods

Reduced density matrix algorithms such as the ACSE do not depend on the N-electron wave function as opposed to more traditional electronic structure methods. While a wave function solution is required to initialize the ACSE algorithm by providing an approximate 2-RDM, the ACSE is subsequently solved via the procedure outlined above which relies solely upon the 1- and 2-RDMs to reconstruct the 3-RDM and the cumulant 3-RDM. Further use of a wave function is not required. In doing so, the problem is reduced from an N-body problem to a 2-body problem [23, 24]. Both single and multi-referenced approaches can be used to generate this initial 2-RDM input. However, because the ACSE is a minimization scheme, its accuracy greatly depends on the appropriateness of the initial wave function approximation.

The multi-configuration self consistent field (MCSCF) method is typically used to generate an initial wave function guess for the ACSE when examining strongly-correlated systems. Unlike a single referenced method this multi-reference active space approach provides the ACSE algorithm with excited state determinants that better describe the ground state virtual orbitals. Despite this advantage, MCSCF is a post Hartree-Fock active space method and therefore the core orbitals (those that are doubly occupied and not in the active space) remain uncorrelated [25]. One of the major advantages of the ACSE is that it can re-correlate these core electrons and recapture the lost core-core and core-active electronic correlation energies. The result is a more balanced treatment of correlation energy effects than that of an MCSCF solution alone.

Like the ACSE, perturbation theory can be applied to the result of single [26] or multi-referenced [27] methods as well as both ground and excited states to improve the result for a greater computational cost. Møller Plesset perturbation scales as N^5 (where N is the number of electrons) after an MCSCF calculation provides the initial wave function, which already required exponential scaling [28]. Application of perturbation theory to the single-referenced

hierarchy of coupled cluster routines increases the scaling by one order of magnitude. Where coupled-cluster singles and doubles (CCSD) scales as N^6, the 'golden standard' electronic calculation of CCSD with perturbative triples (CCSD(T)) sclaes as N^7 [29]. In contrast the ACSE scales as $r_a^2 r_e^4$ when initiated with a multi-referenced guess and attains impressive accuracy as will be shown in later chapters. Additionally, perturbation theory will only be of use when any changes in the investigated system are minimal. Even then, this approach lacks an iterative scheme and does not necessarily converge.

2.4.2 Comparison to the CSE

As previously discussed, the CSE and HCSE both depend on the 3- and 4-RDM whereas the ACSE only relies on the 3-RDM and thus we only need to reconstruct one additional RDM [7, 17]. Moreover, the 3-RDM term in the ACSE expression in Eqn. 2.14 only appears as a factor on the perturbative terms of the 2-electron integral of the reduced Hamiltonian. The accuracy of the final solution depends directly upon the accuracy of that single reconstruction, which only requires first order terms for the ACSE case using the Mazziotti scheme in Eqn. 2.20. That is to say, the first order 3-RDM reconstruction for the ACSE yields a 2-RDM solution that is correct through second order. The 3-RDM reconstruction for the HCSE and the full CSE requires second order correction terms to attain similar accuracy. Even with a second order 3-RDM reconstruction for these two latter approaches, there is still the matter of the 4-RDM reconstruction. This requires even further approximation and subsequent compounded errors.

Additionally, the 2-RDM computed by the CSE must be purified at each step in the iteration in order to maintain N-representability. This purification takes the form of enforcing the known N-representability constraints for the 1-, 2- and 3-RDMs. At each step the relevant RDMs must be checked for positive-semidefiniteness and possess the appropriate trace values [2, 4].

2.5 References

[1] D. A. Mazziotti, "Quantum chemistry without wave functions: two-electron reduced density matrices.," *Acc. Chem. Res.*, vol. 39, pp. 207–15, mar 2006.

[2] D. A. Mazziotti, "Variational method for solving the contracted Schrödinger equation through a projection of the N-particle power method onto the two-particle space," *J. Chem. Phys.*, vol. 116, pp. 1239–1249, jan 2002.

[3] M. Mihailović and M. Rosina, "The variational approach to the density matrix for light nuclei," *Nucl. Phys. A*, vol. 237, pp. 221–228, jan 1975.

[4] D. R. Alcoba and C. Valdemoro, "Spin structure and properties of the correlation matrices corresponding to pure spin states: Controlling the S-representability of these matrices," *Int. J. Quantum Chem.*, vol. 102, no. 5, pp. 629–644, 2005.

[5] R. M. Erdahl, "Representability," *Int. J. Quantum Chem.*, vol. 13, pp. 697–718, jun 1978.

[6] D. A. Mazziotti, "Two-electron reduced density matrix as the basic variable in many-electron quantum chemistry and physics.," *Chem. Rev.*, vol. 112, pp. 244–62, jan 2012.

[7] C. Valdemoro and D. R. Alcoba, *Frontiers in Quantum Systems in Chemistry and Physics*, vol. 18 of *Progress in Theoretical Chemistry and Physics*. Dordrecht: Springer Netherlands, 2008.

[8] D. A. Mazziotti, "Approximate solution for electron correlation through the use of Schwinger probes," *Chem. Phys. Lett.*, vol. 289, pp. 419–427, jun 1998.

[9] D. A. Mazziotti, "Anti-Hermitian part of the contracted Schrödinger equation for the direct calculation of two-electron reduced density matrices," *Phys. Rev. A*, vol. 75, p. 022505, feb 2007.

[10] R. McWeeny, "Some recent advances in density matrix theory," *Rev. Mod. Phys.*, vol. 32, pp. 335–369, apr 1960.

[11] G. Gidofalvi and D. A. Mazziotti, "Direct calculation of excited-state electronic energies and two-electron reduced density matrices from the anti-Hermitian contracted Schrödinger equation," *Phys. Rev. A*, vol. 80, p. 022507, aug 2009.

[12] E. J. Sturm and D. A. Mazziotti, "Highly accurate excited-state energies from direct computation of the 2-electron reduced density matrix by the anti-Hermitian contracted Schrödinger equation," *Mol. Phys.*, vol. 114, pp. 335–343, sep 2015.

[13] J. J. Foley, A. E. Rothman, and D. A. Mazziotti, "Strongly correlated mechanisms of a photoexcited radical reaction from the anti-Hermitian contracted Schrodinger equation.," *J. Chem. Phys.*, vol. 134, p. 034111, jan 2011.

[14] D. A. Mazziotti, "Multireference many-electron correlation energies from two-electron reduced density matrices computed by solving the anti-Hermitian contracted Schrödinger equation," *Phys. Rev. A*, vol. 76, p. 052502, nov 2007.

[15] D. A. Mazziotti, "Anti-Hermitian Contracted Schrödinger Equation: Direct Determination of the Two-Electron Reduced Density Matrices of Many-Electron Molecules," *Phys. Rev. Lett.*, vol. 97, p. 143002, oct 2006.

[16] D. A. Mazziotti, "Contracted Schrödinger equation: Determining quantum energies and two-particle density matrices without wave functions," *Phys. Rev. A*, vol. 57, pp. 4219–4234, jun 1998.

[17] D. A. Mazziotti, "Two-electron reduced density matrices from the anti-Hermitian contracted Schrodinger equation: enhanced energies and properties with larger basis sets.," *J. Chem. Phys.*, vol. 126, p. 184101, may 2007.

[18] F. Colmenero and C. Valdemoro, "Approximating q -order reduced density matrices in terms of the lower-order ones. II. Applications," *Phys. Rev. A*, vol. 47, pp. 979–985, feb 1993.

[19] H. Nakatsuji and K. Yasuda, "Direct determination of the quantum-mechanical density matrix using the density equation.," *Phys. Rev. Lett.*, vol. 76, pp. 1039–1042, feb 1996.

[20] K. Yasuda and H. Nakatsuji, "Direct determination of the quantum-mechanical density matrix using the density equation. II.," *Phys. Rev. A*, vol. 56, pp. 2648–2657, oct 1997.

[21] D. A. Mazziotti, "Pursuit of N-representability for the contracted Schrödinger equation through density-matrix reconstruction," *Phys. Rev. A*, vol. 60, pp. 3618–3626, nov 1999.

[22] D. A. Mazziotti, "Complete reconstruction of reduced density matrices," *Chem. Phys. Lett.*, vol. 326, pp. 212–218, aug 2000.

[23] A. Coleman, "The structure of fermion density matrices," *Rev. Mod. Phys.*, vol. 175, no. 35, pp. 668–687, 1962.

[24] C. A. Coleman and V. I. Yukalov, *Reduced Density Matrices: Coulson's Challenge*. Springer, 2000.

[25] M. W. Schmidt and M. S. Gordon, "The construction and interpretation of MCSCF wavefunctions.," *Annu. Rev. Phys. Chem.*, vol. 49, pp. 233–66, jan 1998.

[26] P. G. Szalay and R. J. Bartlett, "Multi-reference averaged quadratic coupled-cluster method: a size-extensive modification of multi-reference CI," *Chem. Phys. Lett.*, vol. 214, pp. 481–488, nov 1993.

[27] W. D. Laidig and R. J. Bartlett, "A multi-reference coupled-cluster method for molecular applications," *Chem. Phys. Lett.*, vol. 104, pp. 424–430, feb 1984.

[28] K. Hirao, "Multireference MøllerPlesset method," *Chem. Phys. Lett.*, vol. 190, pp. 374–380, mar 1992.

[29] A. I. Krylov, "Equation-of-motion coupled-cluster methods for open-shell and electronically excited species: the Hitchhiker's guide to Fock space.," *Annu. Rev. Phys. Chem.*, vol. 59, pp. 433–62, jan 2008.

CHAPTER 3

COMPARISON OF PREDICTED ENERGIES FOR *AB INITIO* METHODS: THE ANTI-HERMITIAN CONTRACTED SCHRÖDINGER EQUATION AND WAVE FUNCTION APPROACHES

This chapter contains parts of an article that was originally published in Molecular Physics. Reprinted with permission from [E. J. Sturm and D. A. Mazziotti, *Mol. Phys*, **114**, 335 (2015)].

3.1 Introduction

Electronically excited states play a pivotal role in numerous chemical processes from photochemistry [1–4] to transition states and biochemistry [5, 6]. However, ground state calculations are far more accessible due to the challenges that excited-state calculations present [7]. In many excited states strong multi-referenced correlation caused by near degeneracies in molecular orbital energies contributes significantly to the wave function description. As a consequence, mean-field solutions are often insufficient as excited-state references [8, 9] since they do not properly model the strong correlation contributions. Full configuration interaction (FCI) calculations by definition capture strong multi-reference correlation effects, but because their computational costs scale exponentially with the number N of electrons, such calculations are generally prohibitive for systems with greater than 12-16 electrons. The design and testing of methods that are capable of reproducing near-FCI accuracy for electronically excited states with polynomial scaling is therefore important.

A variety of *ab initio* techniques have been developed over the last few decades to address this problem. Single-referenced ground-state methods often generate excited states by coupling their ground-state solutions to weak electronic fields and measuring the re-

sponse [1, 6, 10, 11]. These techniques, however, generally have difficulty with excited states because the initial mean-field approximation is a poor descriptor of the virtual orbitals that become populated upon excitation. For this reason multi-referenced approaches with the capability of describing degenerate or near-degenerate orbitals often have greater success with excited-state calculations [12, 13]. Yet these methods can be computationally expensive with exponential scaling when the reference is expressed with determinants and high-order polynomial scaling when the reference is expressed with high-order density matrices.

In addition to more traditional single and multi-referenced wave function approaches there are also reduced density matrix (RDM) methods. Because the N-electron wave function contains more information than is necessary for property computations, it is possible to reduce the degrees of freedom in the problem by contracting the wave function onto the 2-electron space [14, 15]. A stationary condition for ground and excited states can be obtained by contracting the Schrödinger equation onto the 2-particle space to obtain the two-electron contracted Schrödinger equation (CSE) [16–21]. One approach to solving the CSE is known as the ACSE which can be solved for both ground- and excited-state energies as well as 2-RDMs [4, 22].

The indeterminacy of the anti-Hermitian part of the CSE (ACSE) can be removed by reconstructing the 3-RDM from the 2-RDM by its cumulant expansion [23–26]. The cumulant reconstruction of the 3-RDM in the ACSE generates a system of equations that depends only on the 2-RDM. The cumulant approximation is correct through second order in the 2-RDM of a renormalized perturbation theory, and it leads to an ACSE method that scales quadratically with the number of orbitals in the active space. Wave function methods based on multi-referenced perturbation theory, configuration interaction, or coupled-pair approximations [27–29] scale exponentially with the number r_a of active orbitals if the reference space is represented by determinants (and to a higher polynomial power of r^a if reduced density matrices are employed). Because of their high cost, these methods beyond MRPT2 are not as widely used as the excited-state wave function methods compared here. Other

recent methods for ground and excited states have adopted the cumulant reconstruction [23–26] of contracted Schrödinger theory [18, 23, 26, 30], including the canonical transformation method [31] and similarity renormalization group [32]. Cumulant reconstruction of the 3-RDM has also been employed in linear-response 2-RDM methods [33–36].

In this work we examine in detail the vertical excitation energies at equilibrium geometries and dissociation curves of hydrogen fluoride, [22, 37] water [9, 38–40] and the nitrogen molecule [13, 37, 41–44] using single-referenced, multi-referenced and RDM (ACSE) approaches. The purpose of the work is to provide a systematic comparison for ground and excited states calculations of the 2-RDM-based ACSE method with some of the most common wave-function-based methods including multi-configurational self consistent field (MCSCF) [45], multi-reference second order perturbation theory (MRPT2) [46, 47], configuration interaction singles (CIS) [5–7], equations of motion coupled cluster singles and doubles (EOM-CCSD) [10], and time-dependent density functional theory (TD-DFT) [1, 6] with the B3-LYP xc functional [48]. Data from the HF, H_2O and N_2 molecules obtained using the aforementioned methods are directly compared to full configuration interaction (FCI) results. We present and analyze the ACSE results for more excited states and non-equilibrium data for these molecules than in previous work [22]. The variation in electronic excitation and molecular geometry provides an array of criteria by which we investigate *ab initio* methods in their treatment of strong electronic correlation effects.

3.2 Applications

In this section, after discussing the computational details used in this study, we present the equilibrium vertical excitation energies as well as dissociation potential energy curves for HF, H_2O and N_2. Results from the aformentioned wave function approaches (MCSCF [45], MRPT2 [46, 47], CIS [5–7], EOM-CCSD [10], and TD-DFT [1, 6] with the B3-LYP xc functional [48]), and the RDM based ACSE are compared to full configuration interaction (FCI) energies where possible. The ground-state energies of CIS are the Hartree-Fock energies.

3.2.1 Computer Methodology

For all three molecules we use the correlation-consistent polarized valence double-ζ (cc-pVDZ) basis set [49]; in the case of water we further augment this basis set with diffuse functions [39]. Hartree-Fock mean field geometry optimizations are used for the equilibrium configurations in all methods. The equilibrium bond lengths are 0.901Å and 1.077Å for HF and N_2 respectively. For water, R_{OH} is 0.946Å and $\angle A_{HOH}$ is 104.5°.

We employ an MCSCF approach known as the complete active-space self-consistent-field (CASSCF) method [45, 50] to provide initial determinants for MRPT2 and the initial 2-RDM guess for ACSE. The notation used in this work is [X,Y] where X and Y are the number of electrons and spatial orbitals respectively in the active space. CASSCF active spaces are [6,6] for both HF and H_2O and [8,7] [42] for N_2. State averaging is required for some excited states to converge [8]. The CASSCF, MRPT2, CIS, TD-DFT, EOM-CCSD, and FCI calculations were performed using the GAMESS electronic structure package [51]. All 2-RDM computations were performed using the authors' codes.

3.3 Results

3.3.1 Vertical Excitations

In addition to the ground states, the several low-lying excited singlet states were computed for each system: three for HF, eight for H_2O and six for N_2. The HF $B\ ^1\Sigma^+$ state required state averaging in order to converge (0.05:0.95, $\tilde{X}\ ^1\Sigma^+$:$B\ ^1\Sigma^+$). For water, state averaging was required for $2\ ^1B_1$ (0.1:0.9, $1\ ^1B_1$:$2\ ^1B_1$), $3\ ^1A_1$ (0.1:0.9, $2\ ^1A_1$:$3\ ^1A_1$) and $2\ ^1B_2$ (0.1:0.9, $1\ ^1B_2$:$2\ ^1B_2$). All predictions are directly compared to the FCI value as shown in Table 3.1 and Fig. 3.1.

With only a single determinant in the CIS ansätz, states that result from more than one electronic excitation and thus exhibit multi-reference correlation effects have significant errors. Similarly, the coupled cluster (CC) approaches perform best when the state is char-

Table 3.1: The errors of the absolute energy predictions of the ground and several excited singlet states are presented for HF, H_2O and N_2. Results from CASSCF, MRPT2, CIS, EOM-CCSD and ACSE are compared to FCI values (hartrees) in the first column. CIS ground states are mean-field solutions. Ground states are computed with CCSD and corresponding excited states are produced by EOM-CCSD. Excited state geometries have not been re-optimized. *Note:* The ACSE computation for the N_2 $^1\Pi_u$ state required a frozen core orbital treatment. Without the frozen core the error is 17.98 mH.

			$E_{approx} - E_{FCI}$ (mH)				
Molecule	State	FCI (H)	CASSCF	MRPT2	CIS	EOM-CCSD	ACSE
HF	$\tilde{X}\ ^1\Sigma^+$	-100.23020	121.05	11.12	210.49	2.39	0.21
	$^1\Pi$	-99.82496	149.71	12.91	240.15	-1.96	0.63
	$B\ ^1\Sigma^+$	-99.64761	141.19	8.66	251.81	0.41	0.31
	$^1\Sigma^-$	-99.12172	132.93	11.50	286.03	34.92	2.09
H_2O	$1\ ^1A_1$	-76.25753	162.78	10.59	219.73	2.18	-0.88
	$1\ ^1B_1$	-75.98112	137.08	12.41	264.62	-0.47	0.47
	$1\ ^1A_2$	-75.91653	158.28	10.53	262.14	-1.06	-0.83
	$2\ ^1A_1$	-75.89210	163.33	12.37	260.93	-0.39	0.71
	$2\ ^1B_1$	-75.84480	151.62	9.35	257.11	-0.78	-1.53
	$1\ ^1B_2$	-75.82843	168.04	11.46	258.44	-1.07	-0.89
	$3\ ^1A_1$	-75.82215	178.92	9.16	260.01	-0.12	0.16
	$2\ ^1A_2$	-75.79595	162.21	7.90	257.21	0.72	-1.07
	$2\ ^1B_2$	-75.73931	173.74	11.60	237.04	1.10	0.10
N_2	$\tilde{X}\ ^1\Sigma_g^+$	-109.27312	179.39	19.77	317.56	8.98	3.12
	$^1\Pi_g$	-108.91148	205.91	8.07	289.25	11.73	1.90
	$B\ ^1\Sigma_g^+$	-108.88044	206.30	10.53	279.26	13.80	-2.55
	$^1\Sigma_u^+$	-108.86647	220.13	7.15	292.38	15.40	1.06
	$^1\Pi_u$	-108.76595	229.92	2.73	405.72	21.79	3.63
	$C\ ^1\Sigma_g^+$	-108.58727	201.98	9.88	227.04	102.95	1.59
	$^1\Sigma_g^-$	-108.58312	227.18	1.52	222.89	146.82	0.29

acterized by at most single electron excitations. These two single-referenced methods exhibit highly consistent errors for almost every H_2O excited state since they are nearly all singly excited. Notably, CIS and EOM-CCSD have difficulty with the $^1\Sigma^-$ state of HF and all excited states of N_2 as a result of the significantly multi-referenced nature of these states.

As a variational approach, CASSCF predicts energies that are too high due to the lack of stabilizing correlation energy from the inactive orbitals. MRPT2 significantly refines these estimations to a more uniform error of $\sim$10 mH, with one notable exception for the N_2 ground state. The ACSE error range is very similar to that of EOM-CCSD for HF and

water, but unlike EOM-CCSD this degree of error is maintained for all N_2 states except for $^1\Pi_u$ which had an error of 17.98 mH. By freezing the ACSE core orbitals the error was reduced to 3.63 mH as reported in Table 3.1. Overall, MRPT2, EOM-CCSD and ACSE have the most consistent error ranges, but as expected theoretically, EOM-CCSD and ACSE have the greatest quantitative accuracy.

Table 3.2: Vertical excitation energies relative to the ground states from CASSCF, MRPT2, TD-DFT, EOM-CCSD and ACSE are reported and compared to the FCI values (Hartrees), presented in the first column. The ΔE are computed as $\mathrm{E_{excited}} - \mathrm{E_{ground}}$. Then, each method's ΔE is then compared to the FCI's value using $\epsilon = \Delta\mathrm{E_{method}} - \Delta\mathrm{E_{FCI}}$. A negative value indicates that a method's vertical excitation energy is less than the FCI value (i.e., the energy gap is smaller). The B3-LYP functional was used for TD-DFT [48].

			Vertical Excitation Energy Errors (mH)				
Molecule	State	FCI (H)	CASSCF	MRPT2	B3-LYP	EOM-CCSD	ACSE
HF	$^1\Pi$	405.24	28.66	1.79	38.15	-4.34	0.43
	$B\ ^1\Sigma^+$	582.58	20.14	-2.46	-42.72	-1.98	0.11
	$^1\Sigma^-$	1108.47	11.88	0.38	-7.39	32.53	1.88
H_2O	$1\ ^1B_1$	276.41	-25.70	-1.82	-23.57	-2.65	1.35
	$1\ ^1A_2$	341.00	-4.49	-0.06	-35.97	-3.23	0.05
	$2\ ^1A_1$	365.43	0.55	1.78	-33.75	-2.57	1.58
	$2\ ^1B_1$	412.73	-11.16	-1.24	-32.31	-2.96	-0.65
	$1\ ^1B_2$	429.11	5.26	-0.88	-45.91	-3.25	-0.01
	$3\ ^1A_1$	435.38	16.14	-1.43	-25.63	-2.30	1.04
	$2\ ^1A_2$	461.58	-0.57	-2.69	-25.55	-1.46	-0.19
	$2\ ^1B_2$	518.22	10.96	1.01	-51.16	-1.07	0.97
N_2	$^1\Pi_g$	361.64	26.53	-11.70	-7.72	2.75	-1.22
	$B\ ^1\Sigma_g^+$	392.68	26.91	-9.24	-28.49	4.82	-5.67
	$^1\Sigma_u^+$	406.65	40.75	-12.61	-26.61	6.42	-2.06
	$^1\Pi_u$	507.17	50.54	-17.04	15.15	12.81	0.51
	$C\ ^1\Sigma_g^+$	685.85	22.59	-14.10	-92.26	93.97	-1.53
	$^1\Sigma_g^-$	690.00	47.80	-18.25	114.11	137.84	-2.83

The error ε in predicted vertical excitation energies is computed by calculating a method's state vertical excitation energy $\Delta\mathrm{E} = \mathrm{E_{ex}} - \mathrm{E_{gr}}$ and then subtracting the FCI ΔE from that (i.e. error in $\varepsilon = \Delta\mathrm{E_{method}} - \Delta\mathrm{E_{FCI}}$). This allows direct ε comparison between different methods regardless of the absolute state-energy errors shown in Table 3.1. Table 3.2 and image (b) of Fig. 3.1 reports the ε errors from CASSCF, MRPT2, TD-DFT, EOM-CCSD

and ACSE. As before, the inaccuracies for HF and water closely resemble each other whereas those for N_2 varied more. Overall CASSCF ε are too large except for the H_2O transitions $1\ ^1A_1 \rightarrow 1\ ^1B_1, \rightarrow 1\ ^1A_2, \rightarrow 2\ ^1B_1$ and $\rightarrow 2\ ^1A_2$. MRPT2 errors are <2 mH for HF and H_2O due to the consistency in absolute state-energy errors. Larger variations in MRPT2 N_2 absolute state-energies cause greater ε disparities. TD-DFT routinely predicts excitation energies that are too energetically small for all three molecules. The singly excited states from EOM-CCSD are too small with respect to the FCI values, but when the excited states require more excited electrons, the vertical excitations from EOM-CCSD are larger than the FCI values. This occurs in the HF $\tilde{X}\ ^1\Sigma^+ \rightarrow\ ^1\Sigma^-$ transition and all N_2 transitions. The errors in the excitations from the ACSE are consistently small with the exception of $\tilde{X}\ ^1\Sigma^+ \rightarrow B\ ^1\Pi$.

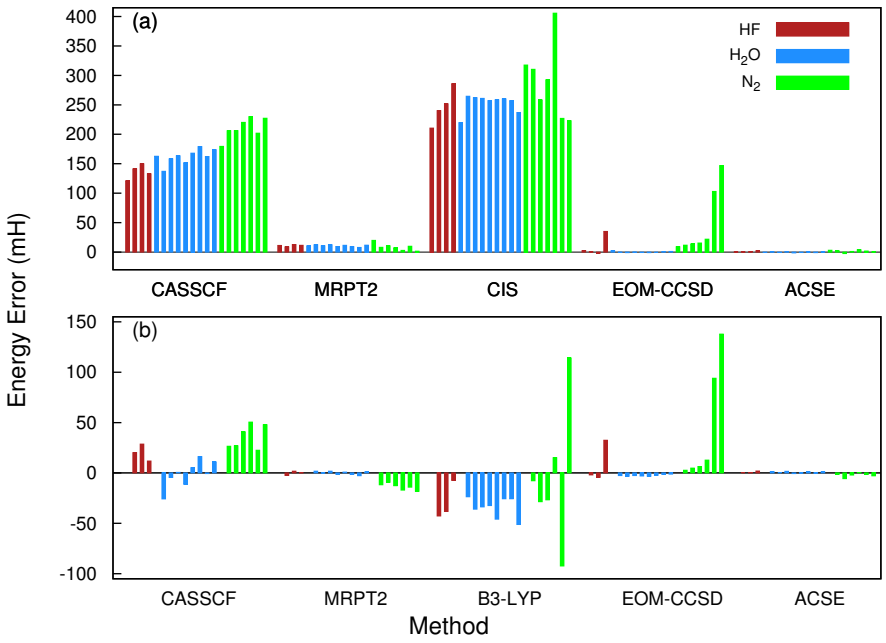

Figure 3.1: Graphic representation energy error comparisons for Tables 3.1 and 3.2. Image (a) shows the absolute energy errors for each state and method in Table 3.1 and image (b) shows the vertical excitation errors for each excited state and method in Table 3.2. The order of the states in each plot corresponds to the order in their respective tables. All errors are measured in millihartrees.

Relative to the FCI results, MRPT2, EOM-CCSD and ACSE provide the most accurate

vertical excitations for HF and H_2O. Of these, MRPT2 and EOM-CCSD exhibit errors with similar orders of magnitude, and ACSE calculations are one to two orders of magnitude closer to the FCI values. MRPT2 has greater difficulty with N_2 as evidenced by the nearly 10 mH range in errors. The EOM-CCSD calculations of the first few excited states of N_2 are very consistent and in two cases the most accurate. However, the $\tilde{X}\ ^1\Sigma_g^+ \rightarrow\ ^1\Sigma_g^-$ and $\rightarrow C\ ^1\Sigma_g^+$ transitions have enormous errors caused by the strongly correlated nature of these states.

3.3.2 Dissociation Curves

The potential energy curves of hydrogen fluoride's ground state ($\tilde{X}^1\Sigma^+$) as well as three excited states ($^1\Pi$, $B^1\Sigma^+$, $^1\Sigma^-$) have been computed in the C_{2v} point group. The $B^1\Sigma^+$ required state averaging for the entire surface (0.05:0.95, $\tilde{X}\ ^1\Sigma^+$:$B\ ^1\Sigma^+$). This state is unique in that it is the only state that is single-referenced when dissociated in this work. Unlike the $^1\Pi$ and $B^1\Sigma^+$ states, $^1\Sigma^-$ requires many doubly excited determinants in its description. Results from EOM-CCSD, MRPT2 and the ACSE at selected geometries are directly compared to FCI data and presented in Table 3.3. Minimum absolute errors are 0.41 mH, 8.08 mH and 0.03 mH for EOM-CCSD, MRPT2 and ACSE respectively. Corresponding maximum absolute errors are 129.69 mH, 13.03 mH and 7.99 mH. Results from CCSD and subsequent EOM-CCSD computations are nearest to the FCI values about equilibrium, even for the strongly multi-referenced $^1\Sigma^-$ state. MRPT2 maintains a fairly consistent error of 8 to 13 mH with respect to the FCI values for all states and geometries. While CC methods typically have better results at equilibrium than MRPT2, the reverse is true upon dissociation and in intermediate regions. In contrast, the ACSE computations exhibit the smallest inaccuracies for every point on the four potential energy curves. Generally, the absolute errors for the ACSE are $\leq$5 mH.

For water, the oxygen and non-dissociative hydrogen atoms are frozen at their equilibrium positions while the other hydrogen is moved in the C_s point group. In Fig. 3.2 we report

Table 3.3: Energetic differences from FCI results of the HF dissociation curves at selected geometries from the EOM-CCSD, MRPT2 and ACSE methods. The equilibrium geometry is $R_0 = 0.901$Å. Negative differences indicate that the method's predicted energy is below the FCI value at that geometry.

			$E_{method} - E_{FCI}$ (mH)		
State	R	FCI (H)	EOM-CCSD	MRPT2	ACSE
$X\ ^1\Sigma^+$	$0.55R_0$	-99.51675	1.67	9.45	0.15
	$1.00R_0$	-100.23020	2.39	11.12	0.21
	$1.55R_0$	-100.13659	4.89	9.62	1.17
	$2.00R_0$	-100.06913	9.73	8.54	0.94
	$2.55R_0$	-100.03727	17.47	8.15	-0.69
	$3.00R_0$	-100.03105	21.39	8.10	-0.03
	$3.55R_0$	-100.02924	23.63	8.08	0.34
$^1\Pi$	$0.55R_0$	-98.98165	-4.56	10.46	0.51
	$1.00R_0$	-99.82496	-1.96	12.91	0.63
	$1.55R_0$	-99.97142	10.19	11.20	0.39
	$2.00R_0$	-100.01064	19.59	11.43	0.01
	$2.55R_0$	-100.02544	26.78	11.03	-0.07
	$3.00R_0$	-100.02821	29.23	11.05	-0.05
	$3.55R_0$	-100.02884	30.38	11.06	-0.04
$B\ ^1\Sigma^+$	$0.55R_0$	-98.76139	-5.18	8.20	0.32
	$1.00R_0$	-99.64761	0.41	8.66	0.31
	$1.55R_0$	-99.76383	16.36	8.90	4.98
	$2.00R_0$	-99.79074	26.81	9.25	1.57
	$2.55R_0$	-99.78105	30.42	8.12	-1.27
	$3.00R_0$	-99.75723	31.24	8.86	-1.07
	$3.55R_0$	-99.72775	32.22	9.28	-1.05
$^1\Sigma^-$	$0.55R_0$	-98.11648	20.56	12.91	7.99
	$1.00R_0$	-99.12172	34.92	11.50	2.09
	$1.55R_0$	-99.44037	94.35	13.03	0.93
	$2.00R_0$	-99.49830	61.20	11.77	0.75
	$2.55R_0$	-99.49266	48.89	10.79	0.77
	$3.00R_0$	-99.47291	51.33	10.51	0.79
	$3.55R_0$	-99.44728	129.69	10.40	0.78

the potential energy curves from EOM-CCSD, MRPT2, and ACSE for the $1A', 1A''$ and $2A'$ states as functions of internuclear distance. The $2A'$ state is state averaged with coefficients of 0.05 and 0.95 for $1A'$ and $2A'$ respectively. While all three states dissociate into the same neutral fragments, the electronic configuration on the oxygen is different in each case. Upon dissociation the $1A''$ excited state ($HO(^2\Pi_z)$) is iso-energetic with the $1A'$ ground

state (HO($^2\Pi_x$)), whereas the higher energy $2A'$ excited state dissociates to HO($^2\Sigma$). Both excited states are the result of single electronic excitations. Multi-reference treatment is required for both excited states at all geometries and the non-equilibrium regime for the $1A'$ ground state.

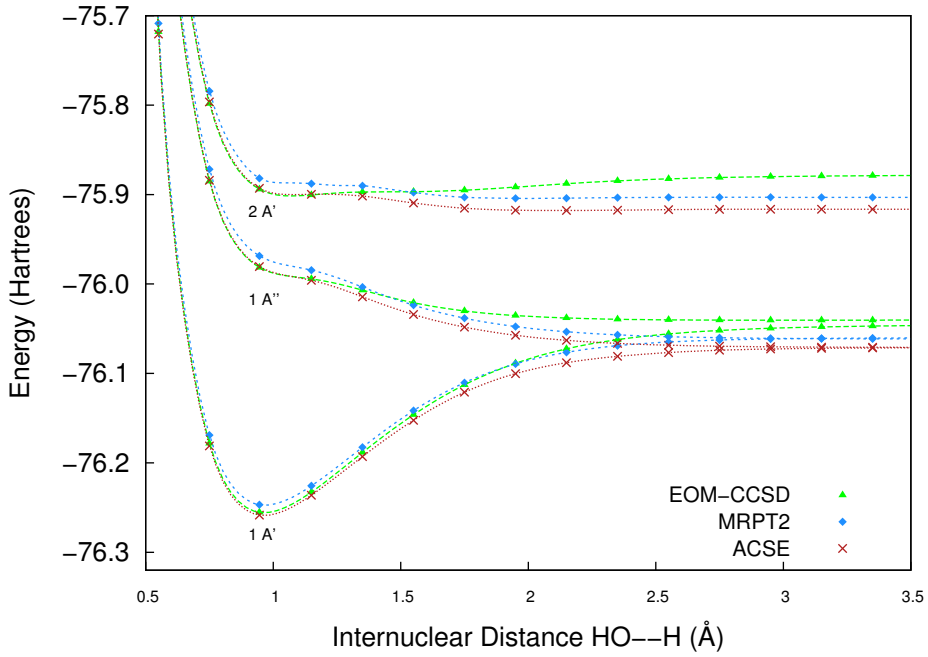

Figure 3.2: Dissociation curves for the H_2O molecule. The ground state $1A'$ (H(^{2}S)+HO($^2\Pi_x$)), and two excited states $1A''$ (H(^{2}S)+HO($^2\Pi_z$))and $2A'$ (H(^{2}S)+HO($^2\Sigma$)) are shown. By mimicking the EOM-CCSD surfaces near equilibrium and MRPT2 upon dissociation, the ACSE exhibits the appropriate treatment of strong multi-reference electronic correlation. MRPT2 remains approximately 10 mH above the ACSE at all geometries in all states.

Examination of Fig. 3.2 reveals that the ACSE better matches the CC results near equilibrium, differing by less than 10 mH. In the non-equilibrium regions the ACSE surfaces qualitatively resemble those of MRPT2, although the energies from these two methods remain different by 9 to 14 mH at all geometries. As the molecule dissociates, EOM-CCSD becomes less suitable and MRPT2 more suitable due to the greater number of determinants required to describe the wave function. Intersections of EOM-CCSD and MRPT2 surfaces occur at 1.7Å, 1.55Å and 1.35Å for $1A'$, $1A''$ and $2A'$ respectively. The surfaces

cross at shorter internuclear distances with the increase of excitation degree. By reproducing the single-referenced EOM-CCSD potential energy curves near equilibrium and the multi-referenced MRPT2 potential energy curves far from equilibrium, the ACSE demonstrates a balanced treatment of strong electronic correlation effects.

Lastly we investigated the $\tilde{X}\ ^1\Sigma_g^+$, $^1\Pi_g$ and $B\ ^1\Sigma_g^+$ states of the nitrogen molecule in the C_{2v} point group. This system's dissociation has been widely studied [13, 41–43] due to the difficulty of modelling the triple bond breakage with the large number of iso-energetic molecular orbitals. Similar to the ground states of HF and H_2O, the $\tilde{X}\ ^1\Sigma_g^+$ ground state is well described by a single determinant at equilibrium and multiple references upon dissociation. The excited states are also multi-referenced at all geometries, and the number of contributing determinants increases as the atoms separate. However, most of the excited determinants in all states require two or more excitations in contrast to all water states and the three lowest states of HF. In Fig. 3.3 we present the potential energy curves from EOM-CCSD, MRPT2 and ACSE computations of $\tilde{X}\ ^1\Sigma_g^+$, $^1\Pi_g$ and $B\ ^1\Sigma_g^+$ (images (c), (b) and (a) respectively) as a function of the internuclear distance between the two N nuclei.

Energetic predictions from CCSD and the ACSE in the immediate equilibrium neighborhood of the ground state are within 10 mH. MRPT2 equilibrium predictions exceed the other two methods by 16 mH or more here, akin to similar discrepancies measured for absolute state energies in Table 3.1 and Fig. 3.1, image (a). As the internuclear distance increases, doubly excited determinants make non-trivial contributions to the wave function description. By 1.3Å the CCSD and MRPT2 have crossed and the ACSE curve qualitatively mimics the MRPT2 at an energetic separation of 9 to 10.5 mH. The CCSD curve begins to show non-physical behavior at 2.0Å and ceases to converge after 2.5Å. Excited-state energies produced by EOM-CCSD are lower than those of MRPT2 only at internuclear distances less than the equilibrium geometry; at larger distances the EOM-CCSD surfaces can be as much as 80 mH greater than the MRPT2 surfaces. At 2.0Å the EOM-CCSD fails to converge, although

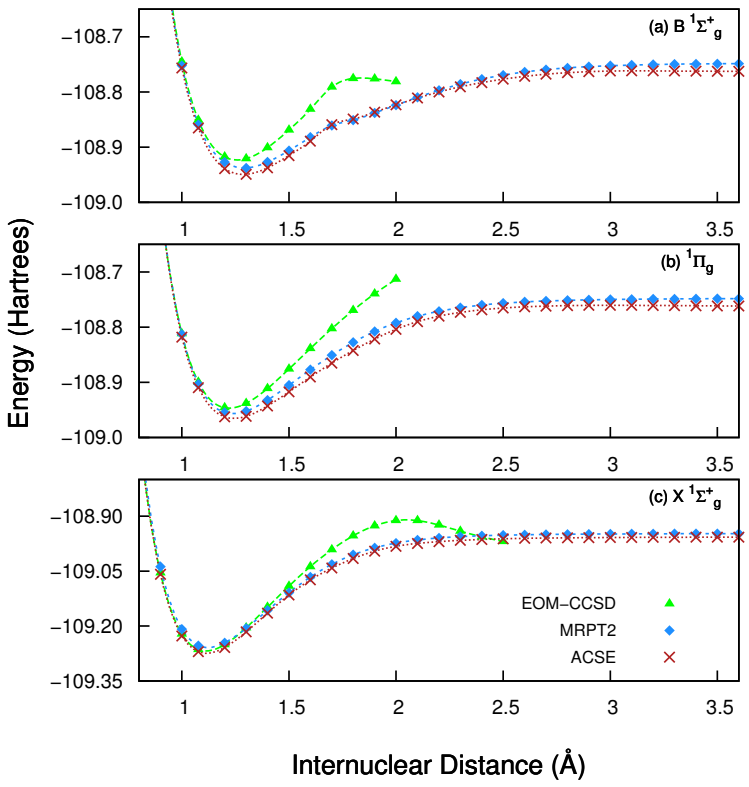

Figure 3.3: Dissociation curves for the N_2 molecule for three states. The ground ($\tilde{X}^1\Sigma_g^+$) (c) and two excited states ($^1\Pi_g$ (b), $B\ ^1\Sigma^+$ (a)) are shown. The CCSD ground state did not converge beyond an internuclear distance of 2.5Å and exhibits the characteristic hump in the potential energy curve. The EOM-CCSD for the excited states was unable to converge beyond 2.0Å. MRPT2 and ACSE qualitatively mimic each other.

the surfaces begin to exhibit divergent behavior ∼1.5Å. The ACSE reproduces the MRPT2 excited surfaces 8 to 14 mH below the MRPT2 save one location where the MRPT2 is lower than the ACSE. The $B\ ^1\Sigma_g^+$ state has an interesting "bump" feature at 1.7Å in the potential energy curves with all three methods. A similar bump was observed by Engels-Putzka and Hanrath in Ref. [41]. At this geometry the coefficient for the ground-state electron configuration abruptly becomes much larger compared to its role at the previous geometry and it contributes more to the overall wave function description.

3.4 Discussion and Conclusions

A variety of *ab initio* methods including the 2-RDM-based ACSE and widely used wave function methods were applied to hydrogen fluoride, water and the nitrogen molecule to assess the methods' treatment of strong multi-reference correlation, especially the correlation appearing in excited states and/or non-equilibrium states. These molecules permit systematic comparisons with FCI. The ACSE calculations for these molecules are more extensive than those previously reported [22, 37].

The ACSE begins with the same initial information as MRPT2, namely a CASSCF wave function, but because the ACSE employs a renormalization of conventional perturbation theory through its cumulant reconstruction, it significantly improves the energetic predictions of MRPT2. When FCI data is available, the ACSE consistently exhibits absolute errors usually <2 mH, the minimum amongst all methods tested regardless of state or system geometry. In contrast, the next most quantitatively accurate method is the EOM-CCSD, predicting energies within 5 mH of the FCI. However, this is only the case when the system is near equilibrium geometry and additional reference determinants are singly excited at most. Situations where double or more excitations are predominant cause the EOM-CCSD to have greater inaccuracies.

Although MRPT2 absolute energies do not attain the same accuracy as EOM-CCSD, the MRPT2 calculations in this work provide consistent data that qualitatively resemble the FCI results where available. MRPT2 energetic prediction errors typically range from 8 to 14 mH above the FCI values, but there is no iterative scheme to further improve these results. This is the same energetic separation between MRPT2 and ACSE observed for the majority of this study.

Although the ACSE has been successfully applied to excited states of more complicated systems including the chemistry of conical intersections [4, 52], the present results provide the most systematic study to date on a set of benchmark molecules where FCI can be computed. The comparisons with widely employed excited-state methods show that the ACSE provides

significant accuracy both in the presence and absence of strong multi-referenced electron correlation. Cumulant reconstruction in combination with the ACSE provides a method that can treat chemistry at both equilibrium and non-equilibrium geometries for ground and excited states, thereby opening new possibilities for the computational study of molecular structure and processes.

3.5 References

[1] A. D. Laurent and D. Jacquemin, "TD-DFT benchmarks: A review," *Int. J. Quantum Chem.*, vol. 113, pp. 2019–2039, sep 2013.

[2] H. H. Falden, K. R. Falster-Hansen, K. L. Bak, S. Rettrup, and S. P. A. Sauer, "Benchmarking second order methods for the calculation of vertical electronic excitation energies: valence and Rydberg states in polycyclic aromatic hydrocarbons.," *J. Phys. Chem. A*, vol. 113, pp. 11995–2012, oct 2009.

[3] H. Okabe, *Photochemistry of Small Molecules*. New York: John Wiley & Sons, Inc., 1978.

[4] J. W. Snyder and D. A. Mazziotti, "Photoexcited conversion of gauche-1,3-butadiene to bicyclobutane via a conical intersection: energies and reduced density matrices from the anti-Hermitian contracted Schrödinger equation.," *J. Chem. Phys.*, vol. 135, p. 024107, jul 2011.

[5] L. González, D. Escudero, and L. Serrano-Andrés, "Progress and challenges in the calculation of electronic excited states.," *Chemphyschem*, vol. 13, pp. 28–51, jan 2012.

[6] A. Dreuw and M. Head-Gordon, "Single-reference ab initio methods for the calculation of excited states of large molecules.," *Chem. Rev.*, vol. 105, pp. 4009–37, nov 2005.

[7] J. B. Foresman, M. Head-Gordon, J. A. Pople, and M. J. Frisch, "Toward a systematic

molecular orbital theory for excited states," *J. Phys. Chem.*, vol. 96, pp. 135–149, jan 1992.

[8] H. Nakano, "Quasidegenerate perturbation theory with multiconfigurational self-consistent-field reference functions," *J. Chem. Phys.*, vol. 99, no. 10, p. 7983, 1993.

[9] C. W. Bauschlicher and P. R. Taylor, "Benchmark full configuration-interaction calculations on H2O, F, and F," *J. Chem. Phys.*, vol. 85, p. 2779, sep 1986.

[10] A. I. Krylov, "Equation-of-motion coupled-cluster methods for open-shell and electronically excited species: the Hitchhiker's guide to Fock space.," *Annu. Rev. Phys. Chem.*, vol. 59, pp. 433–62, jan 2008.

[11] S. Hirata and M. Head-Gordon, "Time-dependent density functional theory within the TammDancoff approximation," *Chem. Phys. Lett.*, vol. 314, pp. 291–299, dec 1999.

[12] B. O. Roos, M. Szulkin, and M. Jaszuński, "Dynamic correlation for MCSCF wave functions: An effective potential method," *Theor. Chim. Acta*, vol. 71, pp. 375–384, jun 1987.

[13] C. W. Bauschlicher and S. R. Langhoff, "Full CI benchmark calculations on N2, NO, and O2: A comparison of methods for describing multiple bonds," *J. Chem. Phys.*, vol. 86, p. 5595, may 1987.

[14] J. Mayer, "Electron Correlation," *Phys. Rev.*, vol. 100, pp. 1579–1586, dec 1955.

[15] A. Coleman, "The structure of fermion density matrices," *Rev. Mod. Phys.*, vol. 175, no. 35, pp. 668–687, 1962.

[16] H. Nakatsuji, "Equation for the direct determination of the density matrix," *Phys. Rev. A*, vol. 14, pp. 41–50, jul 1976.

[17] L. Cohen and C. Frishberg, "Hierarchy equations for reduced density matrices," *Phys. Rev. A*, vol. 13, pp. 927–930, mar 1976.

[18] F. Colmenero, C. Valdemoro, and C. Pérez del Valle, "Approximating q-order reduced density matrices in terms of the lower-order ones. II. Applications," *Phys. Rev. A*, vol. 47, pp. 979–985, feb 1993.

[19] H. Nakatsuji and K. Yasuda, "Direct Determination of the Quantum-Mechanical Density Matrix Using the Density Equation," *Phys. Rev. Lett.*, vol. 76, pp. 1039–1042, feb 1996.

[20] D. A. Mazziotti, "Contracted Schrödinger equation: Determining quantum energies and two-particle density matrices without wave functions," *Phys. Rev. A*, vol. 57, pp. 4219–4234, jun 1998.

[21] D. A. Mazziotti, "Variational method for solving the contracted Schr??dinger equation through a projection of the N-particle power method onto the two-particle space," *J. Chem. Phys.*, vol. 116, pp. 1239–1249, jan 2002.

[22] G. Gidofalvi and D. A. Mazziotti, "Direct calculation of excited-state electronic energies and two-electron reduced density matrices from the anti-Hermitian contracted Schrödinger equation," *Phys. Rev. A*, vol. 80, p. 022507, aug 2009.

[23] D. A. Mazziotti, "Approximate solution for electron correlation through the use of Schwinger probes," *Chem. Phys. Lett.*, vol. 289, pp. 419–427, jun 1998.

[24] D. A. Mazziotti, "3,5-contracted Schrdinger equation: Determining quantum energies and reduced density matrices without wave functions," *Int. J. Quantum Chem.*, vol. 70, pp. 557–570, jun 1998.

[25] W. Kutzelnigg and D. Mukherjee, "Cumulant expansion of the reduced density matrices," *J. Chem. Phys.*, vol. 110, p. 2800, feb 1999.

[26] D. A. Mazziotti, "Anti-Hermitian Contracted Schrödinger Equation: Direct Determi-

nation of the Two-Electron Reduced Density Matrices of Many-Electron Molecules," *Phys. Rev. Lett.*, vol. 97, p. 143002, oct 2006.

[27] W. D. Laidig and R. J. Bartlett, "A multi-reference coupled-cluster method for molecular applications," *Chem. Phys. Lett.*, vol. 104, pp. 424–430, feb 1984.

[28] P. G. Szalay and R. J. Bartlett, "Multi-reference averaged quadratic coupled-cluster method: a size-extensive modification of multi-reference CI," *Chem. Phys. Lett.*, vol. 214, pp. 481–488, nov 1993.

[29] R. J. Gdanitz and R. Ahlrichs, "The averaged coupled-pair functional (ACPF): A size-extensive modification of MR CI(SD)," *Chem. Phys. Lett.*, vol. 143, pp. 413–420, jan 1988.

[30] K. Yasuda and H. Nakatsuji, "Direct determination of the quantum-mechanical density matrix using the density equation. II.," *Phys. Rev. A*, vol. 56, pp. 2648–2657, oct 1997.

[31] T. Yanai and G. K.-L. Chan, "Canonical transformation theory for multireference problems.," *J. Chem. Phys.*, vol. 124, p. 194106, may 2006.

[32] F. A. Evangelista, "A driven similarity renormalization group approach to quantum many-body problems.," *J. Chem. Phys.*, vol. 141, p. 054109, aug 2014.

[33] D. A. Mazziotti, "Extraction of electronic excited states from the ground-state two-particle reduced density matrix," *Phys. Rev. A*, vol. 68, p. 052501, nov 2003.

[34] J. D. Farnum and D. A. Mazziotti, "Extraction of ionization energies from the ground-state two-particle reduced density matrix," *Chem. Phys. Lett.*, vol. 400, pp. 90–93, dec 2004.

[35] L. Greenman and D. A. Mazziotti, "Electronic excited-state energies from a linear response theory based on the ground-state two-electron reduced density matrix," *J. Chem. Phys.*, vol. 128, p. 114109, mar 2008.

[36] D. R. Alcoba, L. M. Tel, E. Pérez-Romero, and C. Valdemoro, "Convergence and computational efficiency enhancements in the iterative solution of the G-particle-hole hypervirial equation," *Int. J. Quantum Chem.*, vol. 111, pp. 937–949, apr 2011.

[37] D. A. Mazziotti, "Multireference many-electron correlation energies from two-electron reduced density matrices computed by solving the anti-Hermitian contracted Schrödinger equation," *Phys. Rev. A*, vol. 76, p. 052502, nov 2007.

[38] R. J. Buenker and S. D. Peyerimhoff, "Calculations on the electronic spectrum of water," *Chem. Phys. Lett.*, vol. 29, pp. 253–259, nov 1974.

[39] O. Christiansen, H. Koch, P. Jørgensen, and J. Olsen, "Excitation energies of H2O, N2 and C2 in full configuration interaction and coupled cluster theory," *Chem. Phys. Lett.*, vol. 256, pp. 185–194, jun 1996.

[40] O. Christiansen, T. M. Nymand, and K. V. Mikkelsen, "A theoretical study of the electronic spectrum of water," *J. Chem. Phys.*, vol. 113, p. 8101, nov 2000.

[41] A. Engels-Putzka and M. Hanrath, "Dissociating N 2 : a multi-reference coupled cluster study on the potential energy surfaces of ground and excited states," *Mol. Phys.*, vol. 107, pp. 143–155, jan 2009.

[42] W. C. Ermler, A. D. McLean, and R. S. Mulliken, "Ab initio study of valence-state potential energy curves of nitrogen," *J. Phys. Chem.*, vol. 86, pp. 1305–1314, apr 1982.

[43] P. Piecuch, S. A. Kucharski, and K. Kowalski, "Can ordinary single-reference coupled-cluster methods describe the potential energy curve of N2? The renormalized CCSDT(Q) study," *Chem. Phys. Lett.*, vol. 344, pp. 176–184, aug 2001.

[44] S. Veeraraghavan and D. A. Mazziotti, "Global solutions of Hartree-Fock theory and their consequences for strongly correlated quantum systems," *Phys. Rev. A*, vol. 89, p. 010502, jan 2014.

[45] M. W. Schmidt and M. S. Gordon, "The construction and interpretation of MCSCF wavefunctions.," *Annu. Rev. Phys. Chem.*, vol. 49, pp. 233–66, jan 1998.

[46] K. Hirao, "Multireference MøllerPlesset method," *Chem. Phys. Lett.*, vol. 190, pp. 374–380, mar 1992.

[47] K. Andersson, P.-Å. Malmqvist, B. O. Roos, A. J. Sadlej, and K. Wolinski, "Second-order perturbation theory with a CASSCF reference function," *J. Phys. Chem.*, vol. 94, pp. 5483–5488, jul 1990.

[48] A. D. Becke, "Density-functional thermochemistry. III. The role of exact exchange," *J. Chem. Phys.*, vol. 98, p. 5648, apr 1993.

[49] T. H. Dunning, "Gaussian basis sets for use in correlated molecular calculations. I. The atoms boron through neon and hydrogen," *J. Chem. Phys.*, vol. 90, p. 1007, jan 1989.

[50] B. O. Roos, P. R. Taylor, and P. E. Sigbahn, "A complete active space SCF method (CASSCF) using a density matrix formulated super-CI approach," *Chem. Phys.*, vol. 48, pp. 157–173, may 1980.

[51] M. W. Schmidt, K. K. Baldridge, J. A. Boatz, S. T. Elbert, M. S. Gordon, J. H. Jensen, S. Koseki, N. Matsunaga, K. A. Nguyen, S. Su, T. L. Windus, M. Dupuis, and J. A. Montgomery, "General atomic and molecular electronic structure system," *J. Comput. Chem.*, vol. 14, pp. 1347–1363, nov 1993.

[52] J. W. Snyder and D. A. Mazziotti, "Photoexcited tautomerization of vinyl alcohol to acetylaldehydevia a conical intersection from contracted Schrödinger theory," *Phys. Chem. Chem. Phys.*, vol. 14, pp. 1660–1667, jan 2012.

CHAPTER 4

INTERMOLECULAR INTERACTION MOTIVATION AND BACKGROUND

4.1 Introduction

With modern advances in computer technology, computational quantum chemistry has reached a maturity that permits us to look beyond individual atoms and small systems. We now have the ability to investigate larger quantum systems in less time and more detail. These advances have paved the way to studying aspects of chemical phenomena and properties that have previously been passed over as being too expensive or required too fine a resolution. One class of these properties is the study of intermolecular interactions which are generally defined as non-covalent interactions possessing energies an order of magnitude smaller than chemical bonds. Whereas first row element bonding energies can range from several dozen millihartrees to as much as half a hartree [1–3], non-covalent interactions can be on the order of a single millihartree or less [4]. A better understanding of the molecular behavior occurring at this energy level would help elucidate many fields of chemical interest spanning protein formation and interactions including those of DNA helices [5–8], photovoltaics [9, 10], condensed phase interactions [6, 11, 12], and singlet fission [9, 13–15] to name a few.

4.2 Types of Intermolecular Interactions

Broadly, there are three main categories that non-covalent molecular interactions typically get sorted into based upon type of energy contribution: electrostatics (polarizability), induction, and dispersion [16, 17]. Some sources further subdivide these classes depending upon the system's state of electronic excitation or intermolecular separation. In some cases the distance separating the molecules of interest may guide how that particular interaction is

examined and interpreted or mathematically modelled and computed [4].

The electrostatic category is perhaps the most easily understood from a classical mechanics standpoint [18, 19]. This is simply the Coulumbic interaction where negatively charged electrons on one monomer repel those on the other, thus influencing all relative electronic distributions and correlating their movements. With larger separations one can view this interaction as a multipole moment response.

The van der Waals dispersion interaction [20] is a purely quantum property resulting from the correlated electron movement between monomers. For this reason the Hartree-Fock approximation cannot reproduce it [21], and in general single-referenced methods will have difficulty unless subsequent modifications are made. In neutral apolar molecules dispersion manifests as an induced dipole–induced dipole effect, creating an attractive potential between them. Dispersion interactions can also be understood as how the electrons on one moiety respond to the instantaneous fluctuations in electron density on another which are measured via dynamic polarizabilities. The third type of interaction is another quantum property called induction. It is very similar in spirit to dispersion interactions as they both measure the energy that comes of the electron distribution on one molecule in response to another nearby [22]. However, whereas dispersion forces are instantaneous, induction energies are the result of a permanent dipole affecting another molecule. Hence, induction interactions are sometimes referred to as polarization interactions.

Some sources also cite a fourth intermolecular interaction known as exchange correlation [4, 16, 23]. Here, the energy contribution comes about from the effects of an electron tunnelling through a classical barrier to go from one monomer to another. This exchange interaction is not to be confused with the exchange energy for electrons of parallel spin in Hartree-Fock calculations (see Chapter 1). This fourth category is usually given the most attention in symmetry adapted perturbation theory approaches which will be discussed in more detail later in this chapter.

A more chemically intuitive classification system exists as an alternative to the afore-

mentioned energetic classifications. Interactions between neutral moieties can be sorted into hydrogen bond dominant, dispersion force dominant, and a third category which is a mixture of dispersion components and other electrostatic (specifically non-hydrogen bonded) contributions [17, 18, 24]. Charged species interactions are typically classified based upon the charge state and whether or not the system exhibits significant charge transfer behavior. This second classification system is less widely used in electronic structure studies since some electronic structure methods can directly compute properties like induction, whereas hydrogen bonding is less rigorously defined by these approaches.

4.3 Computational Expenses: Basis Set

The initial choice of atomic basis set will have a direct and profound effect on the success and computational effort of the electronic structure calculation. In this section we enumerate the different orbital types and desirable characteristics for the choice in basis set when studying intermolecular forces and energies.

4.3.1 Basis Set Improvements

As a basis grows larger and more complete the results obtained using it will be more accurate; however, we cannot utilize an infinite basis for practical reasons [21]. Over the last several decades many Gaussian-type atomic orbitals have been optimized and are now routinely used in electronic structure calculations as elements of finite bases. The first step to improving the minimal basis set is to increase the number of contracted orbitals composing the inner atomic orbitals. The higher energy orbitals for any given atom are less frequently populated and therefore have fewer constituent contracted Gaussian functions. This provides an easily comprehended classification scheme known as the 'ζ hierarchy' [25, 26]. While most electronic structure packages have double, triple, and quadruple (D, T and Q respectively) ζ quality basis sets built in, there are several higher orders available for select elements [27, 28].

Besides increasing the ζ value there are two additional orbital types that can be included to improve the atomic description even further. The first are polarization orbitals which provide the basis set with orbitals of higher angular momentum, permitting the electron distribution about the nucleus to distort and become spherically asymmetrical. This is particularly useful when describing covalent interactions since the electron density will be greater along internuclear axes than elsewhere. The second group are called diffuse functions. These long-tailed Gaussian additions better describe orbitals far away from the nucleus, beyond the covalent interaction range. Atoms and molecules with larger, more polarizable electron clouds that are easily distorted (i.e. soft systems) can be better described with this latter category [4, 25]. Polarization and diffuse orbitals may be used or alone or together with any ζ-order of basis set.

These improved basis sets do have a price though. As the number of atomic orbitals increases so does the number of molecular orbitals which are typically defined as linear combinations of atomic orbitals (LCAOs). The cost of most electronic structure methods is directly dependent on the number of molecular orbitals. Ideally we would use the smallest finite basis capable of correctly reproducing the desired atomic and subsequent molecular behaviors. The choice of atomic basis set however is not always obvious and relies on the target trait or phenomenon under investigation [27].

4.3.2 Basis Set Choice for Intermolecular Interactions

For intermolecular interactions the orbitals must be capable of expressing electronic density at large distances from the nuclei, beyond the covalent bond radius. In this region the orbitals from each molecule must be able to overlap so that the motion of the electrons can correlate. Without correlated electronic behavior the intermolecular interactions we are so keen to examine would not exist. Another outcome of overlapping orbitals is that the electrons from one molecule experience less nuclear shielding of the other molecule's nuclei. This aspect of orbital overlap is sometimes referred to as electron penetration [16, 18]. A

lack of sufficient electron penetration results in a reduction of the Coulombic attractive force between one monomer's electrons and another's nuclei, if present at all. Furthermore, a tunnelling electron in the case of an exchange interaction (see Section 4.2.1) [4], or even a standard charge transfer would need these orbitals to exit and populate.

Minimal basis set descriptions are insufficiently flexible [4, 29] for intermolecular interaction descriptions and therefore we must incorporate at least one of the basis set improvements enumerated above. Using a higher order ζ basis provides the outer orbitals with extra Gaussian functions as well as the inner orbitals. Because intermolecular interactions predominantly take place in these orbitals, larger values of ζ are a natural first choice for basis set enhancement [4]. In addition this improvement to the resolution of the outer orbitals, polarization orbitals can help us model dispersion [29] and induction interactions. The correlated electron movements between monomers resulting from a permanent or induced dipole frequently result in non-symmetric electron distributions about their respective nuclei. In contrast, diffuse orbitals with their greater radii contribute more to molecular orbital overlap description, which has ramifications for electron penetration and electron movement from one monomer to another [5, 30].

An argument could be made for including all of these basis set improvements for any intermolecular study since they each contribute something different to the molecular description with respect to their interactions with other molecules [31]. However it is important to always bear in mind the system's inherent characteristics such as the absence of a permanent dipole [27]. An apolar molecule with a hard electron distribution may not benefit very much from polarized orbitals and their presence would drive up the cost of the calculation for little improvement.

It should also be noted that all of these orbitals are defined and optimized for individual isolated atoms. They are not necessarily the best choices for molecular bonds or interactions. Only by taking linear combinations of them can we approximate these polyatomic properties [21, 25]. Our choices about which atomic orbitals to use will directly impact how well

those properties are simulated. In Chapter 5 we provide a description of a new approach wherein an atomic orbital basis set is used to define a unique optimized molecular orbital basis set for a given monomer.

4.4 Fragmentation Approaches for Investigating Intermolecular Properties

There are several approaches for studying intermolecular interactions in the literature and we briefly discuss a few of them here. Arguably the most significant challenge with intermolecular studies is the sheer size of the problem. In addition to the possibility of a large number of atoms which would require many basis functions even with a minimal atomic basis set, a large basis set is required to properly represent them as described above; a minimal basis set is simply not enough. Furthermore, traditional wave function methods such as CCSD(T) or CASSCF with exponential scaling with respect to the number of molecular orbitals can make intermolecular interactions grossly intractable.

During the last 50 years computational chemists have come up with innovative ways to circumvent these problems such as localizing the orbitals or using a fragmentation approach. Localization approaches take the system as a whole and then assigns floating spherical Gaussian orbitals (not nucleus-centered) to specific region of the system to capture the density of electron distribution. Then all of the sub-densities are added back together for a complete system description. Fragmentation methods also approach electronic systems by breaking it into smaller fragments and reconstructing the full system from these pieces. Most studies use dimers as exemplars, but they can all be extended to larger clusters. Because the monomer optimized basis set ACSE approach described in Chapter 5 can be categorized as a fragmentation method we focus our attention on those in this summary.

4.4.1 Supermolecular Interaction Energies and Basis Set Superposition Error

Supermolecular studies are the most straightforward and thus we start our overview with them. They do not use a specific electronic structure theory, but rather it is a generic mathematical approach for computing the interaction energy. Here, the overall dimer system (or cluster) is computed as a whole and then the individual constituents are computed in isolation using the same level of theory and basis set [32]. The investigator decides which method they wish to use and therefore the expense of a supermolecular approach will scale accordingly. The interaction energy (E_{int}) is defined as the difference between these two calculations:

$$E_{int} = E_{dimer} - \sum E_{monomer}. \tag{4.1}$$

This formula does not tell us much about the actual nature of the molecular behavior [4], just the interaction energy. Despite this drawback, many intermolecular interaction studies incorporate Eqn. 4.1 as a first step in a more detailed analysis; it is quick and easily executed.

The main drawback with the supermolecular scheme is basis set super position error (BSSE) [30, 32, 33]. BSSE is a computational artifact that occurs with the dimer or other calculation with more than a single monomer [5]. When each monomer's energy is computed in isolation, only its own basis functions are available to it for optimization. However, with the dimer (or cluster) calculation a monomer can utilize not only its own basis functions but those on *other* monomers too. This expansion artificially stabilizes the system, lowering the dimer's energy which has the net result of making the interaction and binding energies seem larger than they are. BSSE is more pronounced at closer intermonomer separations because basis functions overlap more with shorter separations.

To address this problem Boys and Bernardi developed the counterpoise (CP) correction in the 1970s [34]. This correction also requires the computation of the isolated monomers properties, but instead of using only the monomer's basis functions, the basis functions of the

other monomer(s) are included as well by using 'ghost atoms.' Ghost atoms are placed in the same places as the normal atoms of the other monomer(s), but without nuclear or electronic charges; in effect they are empty orbitals [5, 32, 35]. By doing this we can directly determine the stabilization effect of excess orbitals on a single monomer at a time. The artifactual energy can be removed from Eqn. 4.1 and the BSSE corrected, making the overall dimer energy smaller and lowering the absolute energetic values of the interaction and binding energies [32].

For several years there was impassioned discussion about the precision of CP corrections with some literature claiming that it over-corrected the BSSE and had to modified to overcome this failing [33, 36]. However, after several more years and additional studies the debate was put to rest with the conclusion that CP corrections did not over correct in all cases and could be used reliably to account for BSSE for certain systems [37]. Addressing BSSE remains an active area of research today.

4.4.2 Symmetry Adapted Perturbation Theory

One of the best known and most successful approaches to intermolecular interaction studies is symmetry adapted pertrubation theory (SAPT) [4, 16]. Like any perturbation theory (PT) method, SAPT decomposes the electronic Hamiltonian into two parts: an unperturbed base Hamiltonian and a small perturbation potential [38]. Here, the unperturbed Hamiltonian $\hat{H}_0$ is the sum of isolated monomers A and B and their interactions in a dimer setting are the perturbation

$$\hat{H} = \hat{H}_0 + \hat{V}_{AB} = \hat{H}_A + \hat{H}_B + \hat{V}_{AB}. \tag{4.2}$$

The isolated monomers can be computed by a variety of approaches including density functional theory (DFT) calculations, a coupled-cluster approximation or even another routine that utilizes perturbation theory to optimize the system's properties. In the last case SAPT becomes a 'double' perturbation method [4]. The unperturbed wave function however is not

a simple product of the isolated wave functions for A and B; doing that would violate Pauli's exclusion principle. This is easily remedied by applying the anti-symmetry operator to the wave function and then symmetry-adapting the result to make it an eigenfunction of $\hat{H}_0$ again. This gives rise to the name of the method. Because the dimer is never computed this method does not have BSSE.

DFT is a very popular choice for the monomer calculation. Studies with this choice are called SAPT(DFT). While DFT generally has difficultly with long range interactions, making it a poor choice for intermonomer studies by itself, it excels with intramonomer behavior which is precisely what is required for the initial Hamiltonian expression. For descriptions of several variations about how DFT and SAPT are used together we refer to the references [39] and [24].

Another feature of SAPT is that the determination of the different types intermolecular interactions is a nearly effortless process. For example, electrostatic (Coulombic) interaction energies can be interpreted as the first order perturbation correction for the energy of the original unperturbed system (ie, the eigenvalue of $\hat{H}_0$). We can compute a value for this by examining the multipole moments of the monomers. Similar parallels can be drawn for other intermolecular interactions, providing physical explanations for energetic values.

Like CCSD(T), SAPT scales as r^7, where r is the number of orbitals, barring various approximations which may make it as little as r^5 or r^4 in some cases [4]. Despite this cost, the ability to instantly identify the type of interaction make SAPT a very attractive option when investigating intermolecular interactions.

4.4.3 The Active Space Decomposition Method

One of the more recently developed methods for intermolecular interaction studies from is the active space decomposition (ASD) approach [40]. Like SAPT, this method also avoids full dimer computations, relying instead on tensor decomposition. Here, a set of states $\{I\}$ and $\{J\}$ are computed for monomers A and B respectively and their product defines a basis

for the dimer state K as follows:

$$|\Psi_K\rangle = \sum_{IJ} C_{IJ}^K \left[|\Phi_I^A\rangle \otimes |\Phi_J^B\rangle \right] \equiv \sum_{IJ} C_{IJ}^K |\Phi_I^A \Phi_J^B\rangle, \tag{4.3}$$

where the resulting wave function is implicitly anti-symmetrized and its states mutually orthogonal. In essence, this defines a basis capable of expressing the dimer's active space as linear combination of tensor products from the isolated monomer active spaces [15, 40]. While this approximation is exact if we compute all possible states of each monomer, in practice this is not necessary to obtain precise results; only small subset of states from each monomer is necessary since the decomposition expression is sufficient for the diagonalization of the dimer electronic Hamiltonian. This means that the active space used to generate the monomer data is the same size as the active space used for the monomer when included as part of the dimer.

By parametrizing the dimer wave function in this manner, we never need to compute the direct product configurations of Eqn. 4.3 and as a result, significant time savings are to be had. However, for this to be true a rigorous procedure must be defined for the generation of the Hamiltonian matrix elements. This is accomplished by expressing the total Hamiltonian as a product of the normal 2-body Hamiltonian operators and the operators that define each of the monomer's sates. That is,

$$\hat{H} = \frac{(-1)^\rho}{2} \sum_{\alpha \in \mathfrak{A}} \sum_{\beta \in \mathfrak{B}} \hat{E}_\alpha \hat{E}_\beta h_{\alpha,\beta}, \tag{4.4}$$

where $\mathfrak{A}$ and $\mathfrak{B}$ are the sets of annihilation and creation operators in second quantization (see Chapter 2) that express monomer A or B's state respectively. α and β are all the orbital index combinations possible for A and B respectively.

The precision of the ASD method is directly dependent on the number of states present with the initial monomer generation. Should greater precision be desired, a larger number of states can be included with a linear increase in the computational cost scales linearly with

respect to the number of monomer configurations [40, 41]. Like SAPT, the ASD method does not have BSSE and therefore a CP correction in unwarranted. While this method is still relatively new, it has already been successfully applied in a study of the singlet fission phenomenon [15].

4.4.4 General Many-Body Expansion

While monomers of single isolated molecules or atoms would seem to be the natural choice for a fragmentation method, there are situations where a small group of particles makes a better subunit. Physical motivations for this partitioning scheme could include strong polarization interactions or perhaps the fragments are defined in such a way that adjacent subunits overlap share several common nuclei [42, 43]. This may be useful in larger clusters where continuity from one fragment to another is desirable. From a computational standpoint a fragmentation scheme with small clusters of particles instead of each particle being its own fragment may dramatically reduce the computational expense [17]. To reconcile these different types of fragmentation schemes and incorporate additional functionality, the general many-body expansion (GMBE) has been developed [42].

To understand GMBE, we start with the many-body expansion (MBE) method. MBE approximates the total energy of this partitioning scheme as a sum of individual fragments plus all pairwise, three-body and higher order correction terms.

$$E = \sum_{I}^{P} E_I + \sum_{I}^{P} \sum_{J<I} \Delta E_{IJ} + \sum_{I}^{P} \sum_{J<I} \sum_{K<J} \Delta E_{IJK} + \cdots \tag{4.5}$$

where P is the total number of fragments and the correction terms are given by

$$\Delta E_{IJ} = E_{IJ} - E_I - E_J, \tag{4.6}$$

$$\Delta E_{IJK} = E_{IJK} - \Delta E_{IJ} - \Delta E_{IK} - \Delta E_{JK} - E_I - E_J - E_K, \tag{4.7}$$

etc.

If we were to expand the above MBE expression to include all P-body terms, this equation would be exact [17]. Another advantage of this model is that it treats all parts of the system at an equal level of theory, regardless of size or location. Despite this exact formula, we cannot use it in its full form because the number of terms would quickly grow larger than computers can handle. To make Eqn. 4.5 useful, higher order terms must be excised. However, some physical phenomena such as a strongly polarized system require higher orders of energetic correction since the fragment is not discreetly defined. A better fragmentation approach in that case may require several overlapping fragments, which the MBE approach as shown above cannot handle without further modification.

The GMBE method seeks to overcome this issue by building in functionality to permit both types of particles. When the fragments are discreet, the GMBE approximation reduces back to Eqn.4.5 but it can also handle cases where the subunits overlap, all in a self-consistent manner [42]. For a system of P fragments GMBE defines the ground-state energy of a system as

$$E = E^{(1)} + \Delta E^{(2)} + \Delta E^{(3)} + \cdots , \tag{4.8}$$

which is understood as the sum of all lone fragment energies plus any higher order energetic corrections which are given by

$$\Delta E^{(n)} = E^{(n)} - E^{(n-1)}. \tag{4.9}$$

where $E^{(n)}$ is an n-body approximation to the ground state energy. The GMBE then proceeds to take the original monomers and create dimers, trimers, ..., n-mers and create a new basis out of these new overlapping fragments. This procedure scales linearly and is easily run in parallel for efficient computation [17].

4.5 References

[1] S. J. Blanksby and G. B. Ellison, "Bond Dissociation Energies of Organic Molecules," *Acc. Chem. Res.*, vol. 36, pp. 255–263, apr 2003.

[2] A. a. Zavitsas, "The Relation between Bond Lengths and Dissociation Energies of CarbonCarbon Bonds," *J. Phys. Chem. A*, vol. 107, pp. 897–898, feb 2003.

[3] J. N. Israelachvili, *Intermolecular and Surface Forces*. Burlington, MA: Academic Press, Inc., third ed., 2011.

[4] K. Szalewicz, "Symmetry-adapted perturbation theory of intermolecular forces," *Wiley Interdiscip. Rev. Comput. Mol. Sci.*, vol. 2, pp. 254–272, mar 2012.

[5] P. Hobza and R. Zahradnik, "Intermolecular interactions between medium-sized systems. Nonempirical and empirical calculations of interaction energies. Successes and failures," *Chem. Rev.*, vol. 88, pp. 871–897, sep 1988.

[6] M. S. Gordon, D. G. Fedorov, S. R. Pruitt, and L. V. Slipchenko, "Fragmentation Methods: A Route to Accurate Calculations on Large Systems," *Chem. Rev.*, vol. 112, pp. 632–672, jan 2012.

[7] C. D. Sherrill, "Energy component analysis of pi interactions," *Acc. Chem. Res.*, vol. 46, no. 4, pp. 1020–1028, 2013.

[8] Ż. Czyżnikowska, R. Zaleśny, and M. G. Papadopoulos, "Nucleic Acid Base Complexes: Elucidation of the Physical Origins of Their Stability," in *Pract. Asp. Comput. Chem.*, pp. 387–397, Dordrecht: Springer Netherlands, 2009.

[9] J. Lee, P. Jadhav, P. D. Reusswig, S. R. Yost, N. J. Thompson, D. N. Congreve, E. Hontz, T. Van Voorhis, and M. A. Baldo, "Singlet exciton fission photovoltaics.," *Acc. Chem. Res.*, vol. 46, pp. 1300–11, jun 2013.

[10] J. L. Bredas, J. P. Calbert, D. A. da Silva Filho, and J. Cornil, "Organic semiconductors: A theoretical characterization of the basic parameters governing charge transport," *Proc. Natl. Acad. Sci.*, vol. 99, pp. 5804–5809, apr 2002.

[11] R. W. Gora, W. Bartkowiak, S. Roszak, and J. Leszczynski, "Intermolecular interactions in solution: Elucidating the influence of the solvent," *J. Chem. Phys.*, vol. 120, no. 6, p. 2802, 2004.

[12] A. Gavezzotti, "Calculation of Intermolecular Interaction Energies by Direct Numerical Integration over Electron Densities. 2. An Improved Polarization Model and the Evaluation of Dispersion and Repulsion Energies," *J. Phys. Chem. B*, vol. 107, pp. 2344–2353, mar 2003.

[13] M. B. Smith and J. Michl, "Recent advances in singlet fission.," *Annu. Rev. Phys. Chem.*, vol. 64, pp. 361–86, jan 2013.

[14] W.-L. Chan, T. C. Berkelbach, M. R. Provorse, N. R. Monahan, J. R. Tritsch, M. S. Hybertsen, D. R. Reichman, J. Gao, and X.-Y. Zhu, "The quantum coherent mechanism for singlet fission: experiment and theory.," *Acc. Chem. Res.*, vol. 46, pp. 1321–9, jun 2013.

[15] S. M. Parker, T. Seideman, M. A. Ratner, and T. Shiozaki, "Model Hamiltonian Analysis of Singlet Fission from First Principles," *J. Phys. Chem. C*, vol. 118, pp. 12700–12705, jun 2014.

[16] B. Jeziorski, R. Moszynski, and K. Szalewicz, "Perturbation Theory Approach to Intermolecular Potential Energy Surfaces of van der Waals Complexes," *Chem. Rev.*, vol. 94, no. 7, pp. 1887–1930, 1994.

[17] L. D. Jacobson, R. M. Richard, K. U. Lao, and J. M. Herbert, "Efficient monomer-based quantum chemistry methods for molecular and ionic clusters," *Annu. Rep. Comput. Chem.*, vol. 9, pp. 25–58, 2013.

[18] Q. Wang, J. A. Rackers, C. He, R. Qi, C. Narth, L. Lagardere, N. Gresh, J. W. Ponder, J. P. Piquemal, and P. Ren, "General Model for Treating Short-Range Electrostatic Penetration in a Molecular Mechanics Force Field," *J. Chem. Theory Comput.*, vol. 11, no. 6, pp. 2609–2618, 2015.

[19] T. Korona, "Exchange-Dispersion Energy: A Formulation in Terms of Monomer Properties and Coupled Cluster Treatment of Intramonomer Correlation," *J. Chem. Theory Comput.*, vol. 5, pp. 2663–2678, oct 2009.

[20] F. London, "The general theory of molecular forces," *Trans. Faraday Soc.*, vol. 33, no. 0, p. 8b, 1937.

[21] N. S. Szabo, Attila; Ostlund, *Modern Quantum Chemistry: Introduction to Advanced Electronic Structure Theory*. Mineola, New York: Dover Publications, Inc., 1 ed., 1982.

[22] K. U. Lao and J. M. Herbert, "Accurate and Efficient Quantum Chemistry Calculations for Noncovalent Interactions in Many-Body Systems: The XSAPT Family of Methods," *J. Phys. Chem. A*, vol. 119, pp. 235–252, jan 2015.

[23] E. Pastorczak, A. Prlj, J. F. Gonthier, and C. Corminboeuf, "Intramolecular symmetry-adapted perturbation theory with a single-determinant wavefunction," *J. Chem. Phys.*, vol. 143, p. 224107, dec 2015.

[24] G. Jansen, "Symmetry-adapted perturbation theory based on density functional theory for noncovalent interactions," *Wiley Interdiscip. Rev. Comput. Mol. Sci.*, vol. 4, pp. 127–144, mar 2014.

[25] F. Jensen, *Introduction to Computational Chemistry, 2nd Edition*. West Sussex, England: Wiley, 2nd ed., 2007.

[26] J. ezáč and P. Hobza, "Benchmark Calculations of Interaction Energies in Noncovalent Complexes and Their Applications," *Chem. Rev.*, p. acs.chemrev.5b00526, 2016.

[27] D. Feller, "The role of databases in support of computational chemistry calculations," *J. Comput. Chem.*, vol. 17, pp. 1571–1586, oct 1996.

[28] K. L. Schuchardt, B. T. Didier, T. Elsethagen, L. Sun, V. Gurumoorthi, J. Chase, J. Li, and T. L. Windus, "Basis set exchange: A community database for computational sciences," *J. Chem. Inf. Model.*, vol. 47, pp. 1045–1052, may 2007.

[29] S. Tsuzuki, T. Uchimaru, and K. Tanabe, "Basis set effects on the intermolecular interaction of hydrocarbon molecules obtained by an ab initio molecular orbital method: evaluation of dispersion energy," *J. Mol. Struct. THEOCHEM*, vol. 307, pp. 107–118, apr 1994.

[30] A. Kaczmarek, A. J. Sadlej, and J. Leszczynski, "First-order interaction energies and the basis set truncation effects," *Mol. Phys.*, vol. 104, pp. 395–407, feb 2006.

[31] S. Tsuzuki, T. Uchimaru, M. Mikami, and K. Tanabe, "PHYSICS Basis set effects on the calculated bonding energies of neutral benzene dimers : importance of diffuse polarization functions," *Chem. Phys. Lett.*, vol. 252, pp. 206–210, apr 1996.

[32] F. B. van Duijneveldt, J. G. C. M. van Duijneveldt-van de Rijdt, and J. H. van Lenthe, "State of the Art in Counterpoise Theory," *Chem. Rev.*, vol. 94, pp. 1873–1885, nov 1994.

[33] S. Simon, M. Duran, and J. J. Dannenberg, "How does basis set superposition error change the potential surfaces for hydrogen-bonded dimers?," *J. Chem. Phys.*, vol. 105, no. 24, p. 11024, 1996.

[34] S. Boys and F. Bernardi, "The calculation of small molecular interactions by the differences of separate total energies. Some procedures with reduced errors," *Mol. Phys.*, vol. 19, pp. 553–566, oct 1970.

[35] G. Lendvay and I. Mayer, "Some difficulties in computing BSSE-corrected potential surfaces of chemical reactions," *Chem. Phys. Lett.*, vol. 297, pp. 365–373, dec 1998.

[36] D. W. Schwenke and D. G. Truhlar, "Systematic study of basis set superposition errors in the calculated interaction energy of two HF molecules," *J. Chem. Phys.*, vol. 82, no. 5, p. 2418, 1985.

[37] L. A. Burns, M. S. Marshall, and C. D. Sherrill, "Comparing Counterpoise-Corrected, Uncorrected, and Averaged Binding Energies for Benchmarking Noncovalent Interactions," *J. Chem. Theory Comput.*, vol. 10, pp. 49–57, jan 2014.

[38] D. J. Griffiths, *Introduction to Quantum Mechanics*. Upper Sadle River, NJ: Prentice Hall, Inc., 1 ed., 1995.

[39] G. Jansen, A. Hesselmann, H. L. Williams, and C. F. Chabalowski, "Comment on "using Kohn-Sham orbitals in symmetry-adapted perturbation theory to investigate intermolecular interactions" (multiple letters)," jan 2001.

[40] S. M. Parker, T. Seideman, M. A. Ratner, and T. Shiozaki, "Communication: Active-space decomposition for molecular dimers.," *J. Chem. Phys.*, vol. 139, p. 021108, jul 2013.

[41] I. Kim, S. M. Parker, and T. Shiozaki, "Orbital Optimization in the Active Space Decomposition Model," may 2015.

[42] R. M. Richard and J. M. Herbert, "A generalized many-body expansion and a unified view of fragment-based methods in electronic structure theory," *J. Chem. Phys.*, vol. 137, no. 6, p. 064113, 2012.

[43] R. M. Richard and J. M. Herbert, "Many-Body Expansion with Overlapping Fragments: Analysis of Two Approaches," *J. Chem. Theory Comput.*, vol. 9, pp. 1408–1416, mar 2013.

CHAPTER 5

MONOMER-OPTIMIZED BASIS SETS FOR THE COMPUTATION OF INTERMOLECULAR FORCES FROM THE ACSE

In Chapter 3 it was shown that the anti-Hermitian contracted Schrödinger equation (ACSE) is capable of providing exceptionally accurate energetic predictions for strongly correlated systems. Chapter 4 discussed the challenges present in the study of dimers and the related problem of intermolecular interactions as well as several current approaches to solving those issues. In this chapter, we present a novel approach using the ACSE to address these outstanding questions.

5.1 Introduction

Highly accurate descriptions of quantum systems via *ab initio* methods typically engender large computational expenses due to exponential scaling with system size inherent to the more sophisticated models [1, 2]. However, not all electronic interactions play significant roles in chemically interesting phenomena. As many general chemistry students know, photonic excitation, bond formation and breakage, charge transfers and dipole effects are all heavily dominated by the electrons in the valence and other orbitals of similar energy (e.g. HOMO-1, LUMO+1) with larger radii [3]. This is the case with dimer systems where the outermost electrons on each monomer interact more readily with each other than the opposing monomer's core electrons. The interactions of inner orbital electrons play a smaller role in this situation, but their dynamic correlation energy contributions cannot be wholly neglected either. Both correlation types must be addressed.

Similarly, very high energy virtual orbitals are nearly never occupied and thus contribute very little to the overall wave function description. In some cases the energy required to populate some of these high energy orbitals exceeds the ionization energy, making their

inclusion non-physical. Excess orbitals in electronic structure routines are the consequence of using larger atomic orbital basis sets which enable us to describe the wave function in greater detail and precision as described in Chapter 4. However, while several unoccupied orbitals are necessary for electronic structure models [4], incorporating all of these higher energy orbitals improves accuracy by a negligible amount at enormous computational expense. A larger basis set is desirable in order to obtain better expressions of the intermolecular interactions in a dimer or cluster, but an excessive number orbitals often makes such calculations too costly.

This chapter describes a novel approach for investigating intermolecular interactions by focusing computational effort on the most important orbitals in the system. Like other fragmentation methods [5], this approach partitions the system into monomeric subunits which are individually modelled. Then, the total system is rebuilt by combining the fragments with interaction parameters and terms. In brief, our approach starts with the optimization of the isolated monomers and then we trim away excess orbitals on each before combining both monomer subsystems into a dimer [6]. A monomer can be a single atom or molecule; a dimer need not consist of identical monomers. By working with the more tractable monomer subunits we can obtain a correlated description of the inner orbitals free from the influence of the opposing monomer which would only have a minor effect anyway. Removing the least important orbitals at the monomer level ensures that the subsequent dimer calculation will be less expensive, but still retain the orbitals that are most important for the overall system. In essence, we make a monomer-optimized orbital basis set for each unit.

The result is that computational resources do not have to be devoted to re-computing core orbital data or the interactions of excessively high energy orbitals, allowing us to focus our attention on the frontier orbitals and their nearest neighbors. The remainder of this present chapter is devoted to the development and execution of this new electronic structure routine.

5.1.1 Notation and Identities

Before proceeding to the theoretical description of the splicing algorithm we pause here to define and summarize the notation that will be utilized in what follows. Previously used symbols such as ${}^{n}D$ will continue to be used in the usual manner. The total number of electrons in a system will be given by N.

M1 and M2 will be used to indicate a monomer when specificity is required. Subscripts $\mathfrak{M}$ and $\mathfrak{D}$ indicate whether a given matrix is in the monomer or dimer basis respectively. Matrix $\mathbf{S}$ is a normalized atomic orbital (AO) overlap matrix in a given basis; it is real and symmetric. Matrix $\mathbf{C}$ is a coefficient matrix describing the molecular orbitals (MOs) of a system in terms of the underlying AO basis set. This matrix is not necessarily square. These matrices will be used extensively in the descriptions that follow and together they possess the following identity where $\mathbf{I}$ is the identity matrix [4]

$$\mathbf{C}^{\dagger}\mathbf{S}\mathbf{C} = \mathbf{I} \tag{5.1}$$

5.2 Monomer Data Generation

5.2.1 Wave Function and RDM Initialization

We begin our approach to dimer studies by performing a standard ACSE calculation on each isolated gas phase monomer with the following steps [7–9]. A mean-field Hartree-Fock result [10] provides a seed for a complete active space self consistent field (CASSCF) routine and an active space is chosen [1]. An active space is denoted by [X,Y] where X is the number of active space electrons and Y is the number of active spatial orbitals. With a CASSCF approximation, the core orbitals are always doubly occupied and the virtual orbitals beyond the active space are never occupied. Active space orbitals may have partial occupations. This initial wave function computation gives us the coefficient matrix ($\mathbf{C}$) which describes the CASSCF MOs in the AO basis.

The final CASSCF wave function is then contracted (integrated) to produce an initial 2-RDM for the ACSE algorithm to optimize as described in Chapter 2. The ACSE algorithm produces a final 2-RDM that correlates the previously uncorrelated CASSCF defined core and virtual orbitals with those in the active space [11, 12]. Contraction of this optimized 2-RDM, ${}^2\mathbf{D}$, provides us with the 1-RDM, ${}^1\mathbf{D}$ [6]

$$ {}^1D^i_k = \frac{1}{N-1}\sum_{j=1}^{N} {}^2D^{i,j}_{k,j}, \tag{5.2} $$

$$ {}^1D^i_k = \langle \Psi | \hat{a}^\dagger_i \hat{a}_k | \Psi \rangle \, . \tag{5.3} $$

Löwdin named the eigenfunctions of the 1-RDM *natural orbitals* (NOs) [13]. These are a special set of MOs that best describe the system in a basis, chosen by the system. We will use $\mathbf{V}$ to denote this eigenvector matrix. The associated eigenvalues are the occupation numbers of these orbitals and examination of these NO occupation values can reveal whether or not an orbital is correlated. An occupation value of nearly 0 describes a virtual orbital while an occupation number approaching unity indicates a doubly occupied spatial core orbital and thus not strongly correlated. It is expected that the core orbital descriptions and occupations will remain fairly constant when a second monomer is introduced to the system. However, a value significantly different from zero or unity implies a strongly correlated orbital and these occupation values are expected to fluctuate in response to the presence of other electrons from the opposing monomer. Examining these occupation changes can tell us much about the nature of intermolecular interactions in a dimer. We will also use these occupation numbers to make decisions regarding excess orbital truncation, discussed later in this chapter.

At the end of this phase we have three data for a monomer: the CASSCF $\mathbf{C}$ matrix from the wave function initialization and eigenvector matrix $\mathbf{V}$ with the corresponding eigenvalues. By using all of these data together, we can define a smaller set of MOs to describe each monomer.

5.2.2 Orbital Truncation: Creation of a Monomer Optimized Basis

As the AO basis set gets larger and therefore more complete and accurate, the number of MOs also increases [10]. Because most electronic structure methods scale with the number of MOs, these larger basis sets can make accurate chemical system calculations extremely costly and unwieldy, if possible at all. To address this issue we use a large AO basis set and remove NOs that do not significantly contribute to the wave function based on occupation number. A very low NO occupation number would imply that the corresponding orbital may be a good candidate for removal. In contrast, a greater occupation value would indicate that the orbital is very important and should be kept for subsequent calculations.

At the end of the monomer ACSE optimization procedure we obtained the 1-RDM which can be understood as a coefficient matrix for the NOs in the basis of CASSCF defined MOs. That is, the NOs are linear combinations of the wave function MOs which are linear combinations of the original AO basis. To express the NOs in terms of the AOs we perform the following matrix algebra:

$$\mathbf{T} \bullet \mathbf{V} = \mathbf{C}^{\circ}_{\mathfrak{M}X} \tag{5.4}$$

where $\mathbf{T} \in \mathbb{R}^{AO\text{x}MO}$ is the coefficient matrix of the MOs in the AO basis, $\mathbf{V} \in \mathbb{R}^{MOxNO}$ is the 1-RDM eigenvector matrix of NOs and $\mathbf{C}^{\circ} \in \mathbb{R}^{AO\text{x}NO}$ is the final NO coefficient matrix in the AO basis. The $^{\circ}$ superscript denotes that no orbital truncation has occurred at this stage. The $\mathfrak{M}X$ subscript indicates that this coefficient matrix corresponds to the optimized orbital basis for monomer X for X = 1 or 2.

Now we remove or 'trim' NOs deemed excessive. While any number of orbitals may be truncated, we typically keep a number of orbitals equal to a smaller basis set [6]. We use the NO occupation number (eigenvalues of the 1-RDM) to determine which orbitals are kept and which are removed; orbitals with the lowest occupations are removed first. For example, if a given basis set A has 20 MOs and a larger basis set B has 35 MOs, we may choose to run the initial steps of this procedure in basis set B and then upon reaching this step, we

remove the 15 NOs with the smallest occupation numbers such that both A and B have an equal number of MOs despite having a different number of AO basis functions. Because $\mathbf{C}^{\circ}$ has dimensions AO x NO this trimming is a simple process of removing columns:

$$\mathbf{C}^{\circ}_{\mathfrak{M}X} \xrightarrow{trim} \mathbf{C}^{p}_{\mathfrak{M}X} \tag{5.5}$$

where p is the number of remaining or kept orbitals, $\mathbf{C}^{\circ}_{\mathfrak{M}X} \in \mathbb{R}^{AO\text{x}NO}$, and $\mathbf{C}^{p}_{\mathfrak{M}X} \in \mathbb{R}^{AO\text{x}p}$ for $p < NO$, completing the generation of all necessary data for a single monomer. Note that the number of AOs (rows) never changes. This coefficient matrix maintains the large detailed AO basis, but only keeps the most chemically important MOs, defining a monomer optimized set of orbitals uniquely selected by the system itself. The ACSE method with a CASSCF initial 2-RDM seed scales as $\sim r_a^2 r_e^4$ where the r_a and r_e are the number of active and virtual orbitals respectively, so the reduction in the number of excess orbitals via truncation greatly improves our computation time.

5.3 Initial Dimer Generation

Once we have completed the preceding steps for both monomers we are now ready to create a dimer by splicing together the monomer data. At this stage we have $\mathbf{C}^{p}_{\mathfrak{M}1}$ and $\mathbf{S}_{\mathfrak{M}1}$ from the first moiety and likewise $\mathbf{C}^{q}_{\mathfrak{M}2}$ and $\mathbf{S}_{\mathfrak{M}2}$ from the second. The number of remaining orbitals p and q for monomers M1 and M2 respectively need not be the same, even in the case of a homodimer. We begin by creating a super-system (SS) in the monomer basis. Then we rotate the SS from the monomer basis to a dimer basis at a desired geometry.

5.3.1 The Super-System Basis

The initial monomer calculations are executed in isolation and therefore the interactions between them are identically zero. As a result, splicing together monomer data has the same net result as placing the monomers infinitely far apart from one other in a vacuum. The SS

coefficient matrix in the monomer basis $\mathbf{C}_{\mathfrak{M}}$ will take on a pseudo-block matrix form since the sum of both monomers AOs may not be equal the total number of remaining MOs and therefore $\mathbf{C}_{\mathfrak{M}}$ will not be a square matrix. Below we have shown an example where M1 has α and a AOs and MOs respectively and the dimer as a whole has χ AOs in total and j MOs:

$$\mathbf{C}_{\mathfrak{M}} = \begin{pmatrix} \phi_{1,1}^{M1} & \phi_{1,2}^{M1} & \cdots & \phi_{1,a}^{M1} & & & & \\ \phi_{2,1}^{M1} & \phi_{2,2}^{M1} & \cdots & \phi_{2,a}^{M1} & & \mathbf{0} & & \\ \vdots & \vdots & \ddots & \vdots & & & & \\ \phi_{\alpha,1}^{M1} & \phi_{\alpha,2}^{M1} & \cdots & \phi_{\alpha,a}^{M1} & & & & \\ & & & & \phi_{\alpha+1,a+1}^{M2} & \phi_{\alpha+1,a+2}^{M2} & \cdots & \phi_{\alpha+1,j}^{M2} \\ & & & & \phi_{\alpha+2,a+1}^{M2} & \phi_{\alpha+2,a+2}^{M2} & \cdots & \phi_{\alpha+2,j}^{M2} \\ & \mathbf{0} & & & \vdots & \vdots & \ddots & \vdots \\ & & & & \phi_{\chi,a+1}^{M2} & \phi_{\chi,a+2}^{M2} & \cdots & \phi_{\chi,j}^{M2} \end{pmatrix}. \tag{5.6}$$

The AOs on M1 do not contribute to the MO descriptions on M2 and as a result the cross terms in the off-diagonal are zero. This would be the case regardless of the number of orbitals trimmed, if any.

5.3.2 Transformation from the Monomer Basis to the Dimer Basis

At infinite separation the off diagonal terms of $\mathbf{C}_{\mathfrak{M}}$ are identically equal to zero, demonstrating that the moieties have no interaction with each other. However, at closer distances the monomers will begin to interact and the off-diagonal terms will populate. To run the ACSE algorithm on a dimer system at a finite separation, an initial wave function at the same desired geometry must be obtained to create an initial 2-RDM guess with coherence terms. As before, we use the CASSCF procedure to provide this guess wave function. However, the CASSCF procedure itself requires a coefficient matrix, $\mathbf{C}_{\mathfrak{D}}$, which is obtained in the following manner.

A standard Hartree-Fock trial is run for the full dimer in the original AO basis at the desired geometry in order to obtain the atomic overlap matrix $\mathbf{S}_{\mathfrak{D}}^{HF}$, coefficient matrix $\mathbf{C}_{\mathfrak{D}}^{HF}$,

and the electron integral matrices ${}^1\mathbf{K}^{HF}$ and ${}^2\mathbf{V}^{HF}$ for the one and two electron integrals respectively. Because this calculation is at a closer intermonomer radius there are coherence terms in the off-diagonal portions of these overlap and coefficient matrices. Combining $\mathbf{C}_{\mathfrak{D}}^{HF}$ and $\mathbf{S}_{\mathfrak{D}}^{HF}$ with $\mathbf{C}_{\mathfrak{M}}$ we create the rotation matrix $\mathbf{R}$ that permits us to re-express ${}^1\mathbf{K}^{HF}$ and ${}^2\mathbf{V}^{HF}$ in terms of the monomer NO basis. $\mathbf{R}$ is defined as

$$\mathbf{R} = \mathbf{C}_{\mathfrak{M}}^{\dagger}\mathbf{S}_{\mathfrak{D}}\mathbf{C}_{\mathfrak{D}}. \tag{5.7}$$

Essentially, we have now expressed the electron integral information in a new effective AO basis. A new Hartree-Fock approximation is computed with this rotated set of integrals and the result is the coefficient matrix for the CASSCF routine, $\mathbf{C}_{\mathfrak{D}}$. The CASSCF routine optimizes $\mathbf{C}_{\mathfrak{D}}$ with an active number of electrons and orbitals equal to the sum of active electrons and orbitals in the monomers. The CASSCF dimer wave function is contracted, the electron integrals are computed and both are submitted to the ACSE routine which provides the final energy and 2-RDM ${}^2D_{\mathfrak{D}}$ for the finitely separated dimer, concluding the procedure.

5.4 Choice of System and Computational Detail

For our initial tests we chose the $(LiH)_2$ linear dimer [14–17]. This system has a moderate dipole and a very small number of electrons (N = 8) making the first trials with our new method expedient. The covalent bond distance in each monomer is $R_{LiH} = 1.5949$Å [18]. The dimer equilibrium configuration was computed to be $R_0 = \sim 3.4$Å, measured as the distance between either the two H atoms or equivalently, the two Li atoms. See Fig 5.1 below.

We chose to do our calculations with the correlation-consistent polarized valence (cc-pVXZ) hierarchy of AO basis sets where the X value indicates double, triple or quadruple ζ quality (i.e. X = D, T, Q) in this work. We also include two basis sets with diffuse orbital

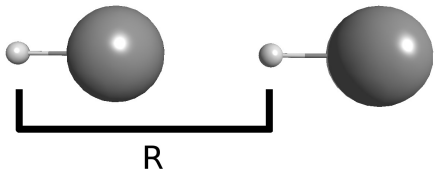

Figure 5.1: An image of the linear $(LiH)_2$ dimer configuration. The intermolecular separation is given by R, which is the distance between the two H atoms or Li atoms. The Li–H bond is frozen at 1.5949Å and the equilibrium intermolecular radius $R_0 = 3.4$Å in this work.

augmentation denoted by the 'aug' prefix: aug-cc-pVDZ and aug-cc-pVTZ [19, 20]. These basis sets were chosen since there they possess a clear progression in size and accuracy and are specifically designed for modelling correlation amongst valence electrons [10]. Furthermore, they will converge systematically to the complete basis set limit when extrapolated. Table 5.1 provides the number of basis functions present in the initial AO and subsequent MO bases for the isolated monomers and combined dimer. Table 5.1 also lists a shorthand for each basis for use in subsequent figures.

Table 5.1: The number of AOs and MOs with spherical harmonics for individual the LiH monomer and $(LiH)_2$ are provided. Because $(LiH)_2$ is a heterodimer, the number of MOs in the total dimer is twice that of a single monomer. Augmented basis sets are denoted by the 'aug' prefix, indicating additional diffuse orbitals.

Basis Set	Abbreviation	AOs	MOs	Dimer MOs
cc-pVDZ	CCD	20	19	38
aug-cc-pVDZ	ACCD	34	32	64
cc-pVTZ	CCT	50	44	88
aug-cc-pVTZ	ACCT	80	69	138
cc-pVQZ	CCQ	105	85	170

All initial wave function calculations (Hartree-Fock, CASSCF) for the monomers are performed with the GAMESS electronic structure package [21]. Subsequent scripts with 2-RDMs (ACSE, basis transformation, truncation) were developed by the author and collaborators.[1] The active spaces for the CASSCF calculations are [2,3] and [4,6] for the monomers and dimer respectively where the first number is active electrons and the second number is the

1. The author wishes to acknowledge the work of A. J. S. Valentine for his contributions to this project.

number of active spatial orbitals. See Chapter 1 for more detail regarding CASSCF.

5.5 Results and Discussion

The dissociation curves and binding energies were computed in each of the five aforementioned basis sets. Every basis set was trimmed down to the sizes of all basis sets with fewer orbitals than it. That is, trials executed in the aug-cc-pVTZ basis set were trimmed from the full number of MOs (138) to 88, 64 and 38 corresponding to the cc-pVTZ, aug-cc-pVDZ and cc-pVDZ bases respectively. In what follows a full, untrimmed and non-monomer-optimized basis set will be denoted by the $^\circ$ symbol next to the number of MOs; for example a full CCT set with 88 MOs will be denoted by CCT (88°) and ACCD (38) indicates that an ACCD trial has been re-optimized and the number of orbitals truncated to a total of 38 MOs.

5.5.1 Dissociation Curves and Binding Energies

Dissociation curves are the potential energy surfaces (PES) that are the result of the total system energy as the constituent monomers are moved closer together from afar. As one would expect, the larger bases obtain more stable and thus, lower energies as shown in Fig. 5.2. As the basis sets become larger and more detailed the relative differences between them begins to decrease, indicating that we are closing in on the true total energy.

In contrast, when we re-optimize and subsequently truncate the monomer bases we observe that the relative ordering of the surfaces are still maintained. An example of all the different truncation levels with the CCQ basis is shown in Fig. 5.3 with the original basis sets for CCD and CCQ. The figure shows that while the CCQ MO basis set has been severely trimmed in some trials, all of their energies are still generally more stable than even ACCT (138°), the next largest full basis set. The only exception to this is the CCQ (38) trial near the equilibrium region, but here the CCQ basis has had 132 MOs removed and the original ACCT basis has 138 total! Similar trends occur with the other bases and their associated

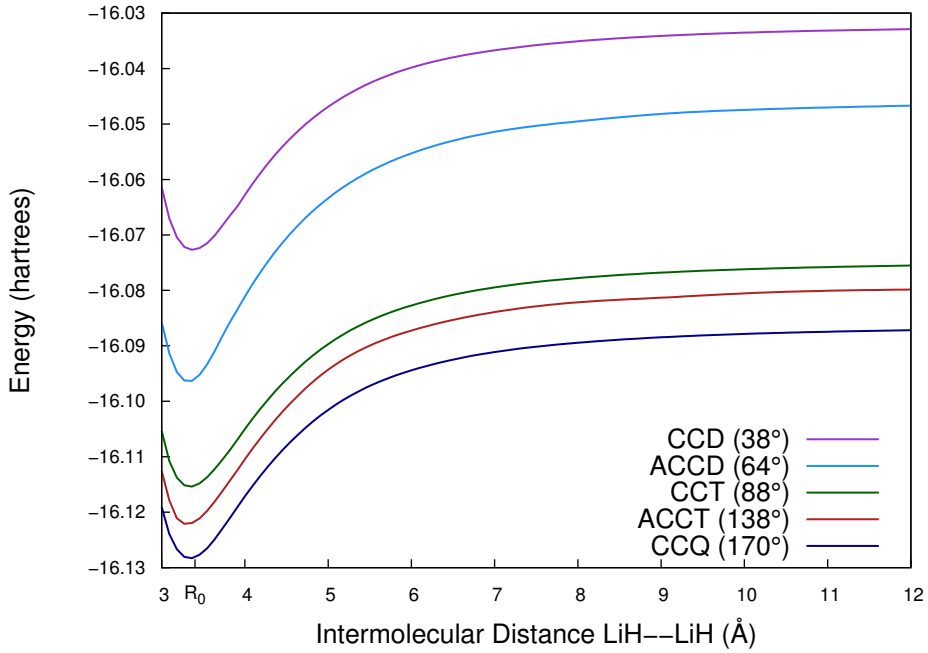

Figure 5.2: The dissociation PES for all basis sets without basis set re-optimization or truncation. The ° symbol indicates that no orbital re-optimization has occurred for that trial. As the basis sets become more complete the system becomes more stabilized and the energetic gaps between them shrinks.

re-optimizations, but they are not shown here.

We can also examine the relative binding energies (BEs) from this data, defined as the energetic difference between the dimer at its equilibrium geometry and at its 'infinite' or largest separation, which in this case is 12.0Å,

$$BE = E(3.4\mathring{A}) - E(12.0\mathring{A}). \tag{5.8}$$

The BE data are shown in Table 5.2. Reading a row across shows us how the BEs changes with respect to different degrees of orbital truncation. Generally the greater the number of MOs trimmed away from a given basis, the more shallow the potential well becomes and as a result the BE also decreases in magnitude. In contrast, by reading down a column we observe how a single basis set responds to truncation after monomer orbital optimization. Unsurprisingly the BE become larger (more negative) as the number of MOs increases down

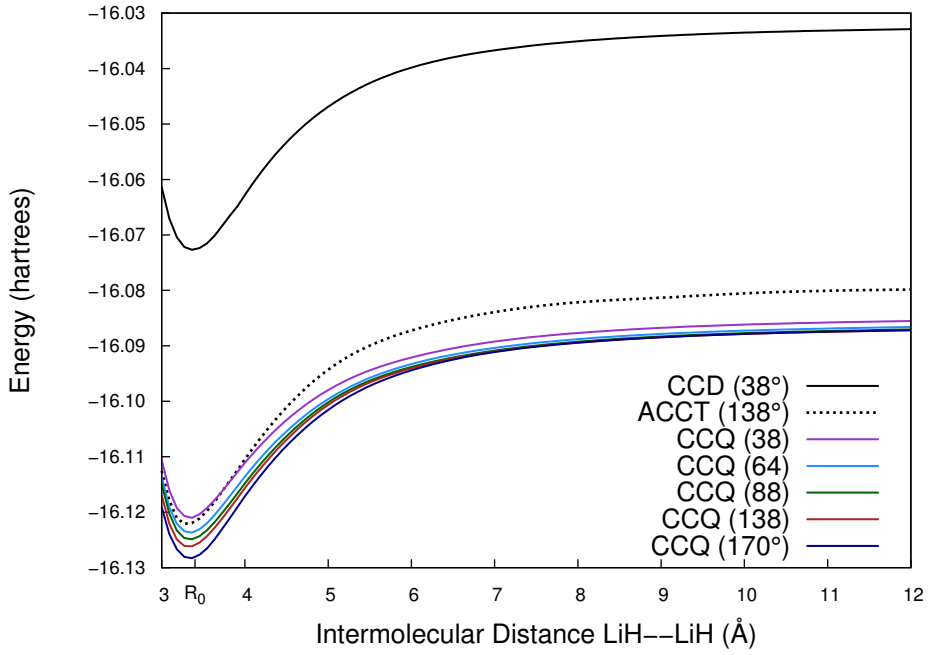

Figure 5.3: Dissociation PES for the original CCD and ACCT basis sets as well as several re-optimized and truncated trials from CCQ. The ° symbol indicates that no orbital re-optimization has occurred for that trial. Generally, the relative ordering of the basis set dissociation curves is maintained.

the table. Most BEs fall between -35 and -40mH, with one notable exception for the true basis set for ACCD at -49.324mH.

Table 5.2: BE of the basis sets with and without monomer orbital optimization. The first entry of each row is the BE of the original dimer system without re-optimization. BEs are defined in Eqn. 5.8. All energies are given in millihartrees.

# MOs	CCD	ACCD	CCT	ACCT	CCQ
38	-39.749	-36.320	-34.890	-35.726	-35.346
64		-49.324	-37.678	-38.964	-36.917
88			-39.719	-39.327	-37.698
138				-41.855	-38.778
170					-40.958

5.5.2 Interaction Energies and Counterpoise Corrections

In addition to the data from dissociation curves we also computed interaction energies (IEs) for each trial in this study. Here we define IE as the difference between the total dimer at a given geometry and the sum of the constituent monomers in isolation:

$$E_{IE} = E_{dimer} - \sum E_{monomer}. \tag{5.9}$$

However, this invites basis set superposition error (BSSE) as discussed in Section 4.4.1, erroneously lowering the IE [22]. This is the condition where a monomer in the dimer calculation is artificially stabilized by the presence of the other monomer's orbitals. This problem is corrected by performing a counterpoise (CP) correction as described by Boys and Bernardi [23, 24]. Each monomer is recomputed in a basis set comprised of not only its own orbitals, but also the orbitals of the opposing monomer without nuclear or electronic charges. In this case the other monomer's place is held by so-called "ghost atoms" which provide the orbitals without the associated charges. The CP corrected IE and the total value for the CP correction (ΔE_{CP}) is given as

$$IE_{CP} = E_{dimer} - E^*_{M1} - E^*_{M2} \tag{5.10}$$

$$\Delta E_{CP} = (E^*_{M1} - E_{M1}) + (E^*_{M2} - E_{M2}) \tag{5.11}$$

where the * indicates that the monomer energy was computed using the dimer basis by way of ghost atoms for the other monomer. The CP energy value will be negative when computed as shown above; it is the artificial stabilization energy gained from BSSE. In addition to the standard IE calculation (Eqn.5.9) we have also performed a CP correction by recomputing each monomer in a ghost atom modified basis set at each geometry. In these cases we select the active space for the CASSCF to be the same size as the original monomer: [2,3].

In Table 5.3 we compare the IE in an analogous fashion to Table 5.2, but unlike before

these IE energies have been CP corrected. As expected, all IE values are less stabilized than their raw uncorrected counterparts, usually by 2-3mH and 4mH in a minority of cases. Most IE values fall between -32 and -38mh, with a single exception for the ACCD (38) trial with an energy of -24.422mh. Interestingly both trials with the ACCD basis set are made ∼12mh less stable with the CP, making the ACCD (64°) trial similar to other trials. Previously ACCD (38) with its uncorrected BE of -36.320mH (Table 5.2) had been considered average, but with CPC it is now the outlier.

Table 5.3: The IE (Eqn. 5.10) curves of the basis sets with and without monomer orbital optimization. As before, the first entry of each row is the IE of the original dimer system without re-optimization. All energies have been CP corrected and are given in millihartrees.

# MOs	CCD	ACCD	CCT	ACCT	CCQ
38	-36.385	-24.422	-33.487	-32.115	-32.775
64		-37.642	-36.193	-34.368	-34.580
88			-38.193	-35.759	-35.440
138				-38.232	-36.457
170					-38.712

In the figures that follow, all IE curves have been adjusted by a constant amount such that the IE is identically equal to 0 at 12.0Å. Fig. 5.4 shows the shifted IE curves with (solid line) and without (broken line) CP corrections for all trials that have been re-optimized and truncated to 38 MOs except for CCD which naturally has 38 MOs. Fig. 5.5 shows the same curves but zoomed into the equilibrium region for closer examination.

While the CP correction is appropriate and necessary for trials with original bases (i.e. those with °), the same cannot be said for the re-optimized bases of our presented method. This is because BSSE occurs as a result of monomers borrowing orbitals from each other. However, our optimized MO bases are created at the monomer level, in the absence of extra orbitals, similar to symmetry adapted perturbation theory (SAPT, see Chapter 4). The subsequent super-system expression also expresses each constituent monomer as an isolated unit (Eqn. 5.6), free from all intermonomer interactions.

Furthermore, closer examination of Fig. 5.5 reveals that the *uncorrected* IE curves are in

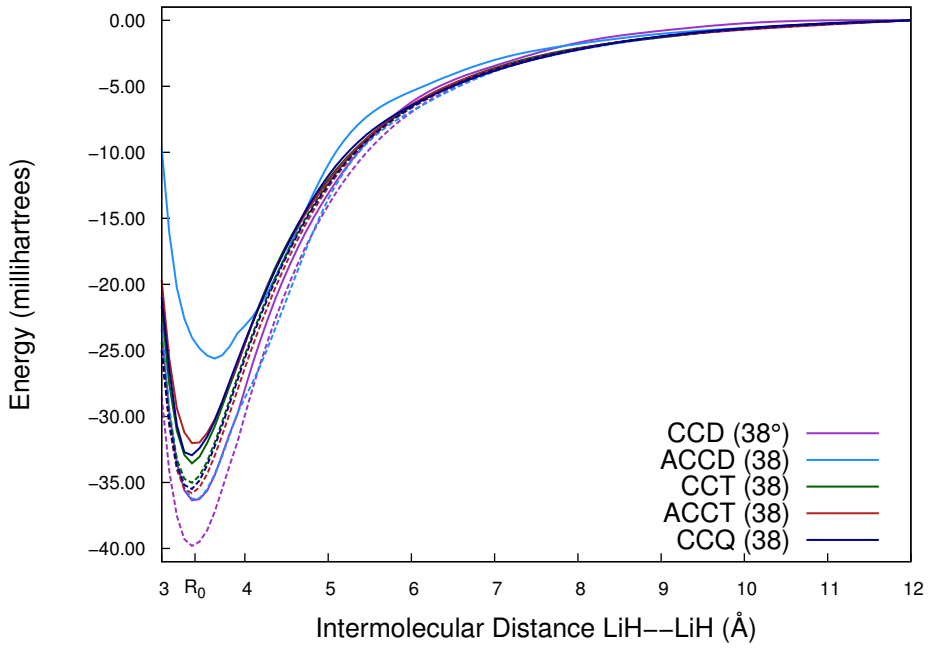

Figure 5.4: IE curves for all bases when re-optimized and truncated to 38 MOs, the same number of MOs as a regular trial with the CCD basis. Solid lines have been counterpoise corrected and broken lines are the uncorrected interaction energies.

fact closer to the true CCD (38°) trial which does require CP correction. This suggests that the optimized orbital basis sets we have developed do not require CP corrections to obtain. Similar trends can be observed at other levels of truncation but they have not been shown here. Table 5.4 shows the CP corrected original bases compared to the uncorrected data computed by the optimized monomer approach. Now the interactions across each row are

Table 5.4: CP corrected original basis BE compared to their IE counterparts after re-optimization and truncation from larger bases. The first value in each row is the CP corrected value for the basis and the remaining energies are the uncorrected values from Tables 5.2 and 5.3 respectively. All energies are given in millihartrees.

# MOs	CCD	ACCD	CCT	ACCT	CCQ
38	-36.385	-36.320	-34.890	-35.726	-35.346
64		-37.642	-37.678	-38.964	-36.917
88			-38.293	-39.327	-37.698
138				-38.232	-38.778
170					-38.712

within ∼1.5mh. This, combined with the original PES of the dissociation curves shown in

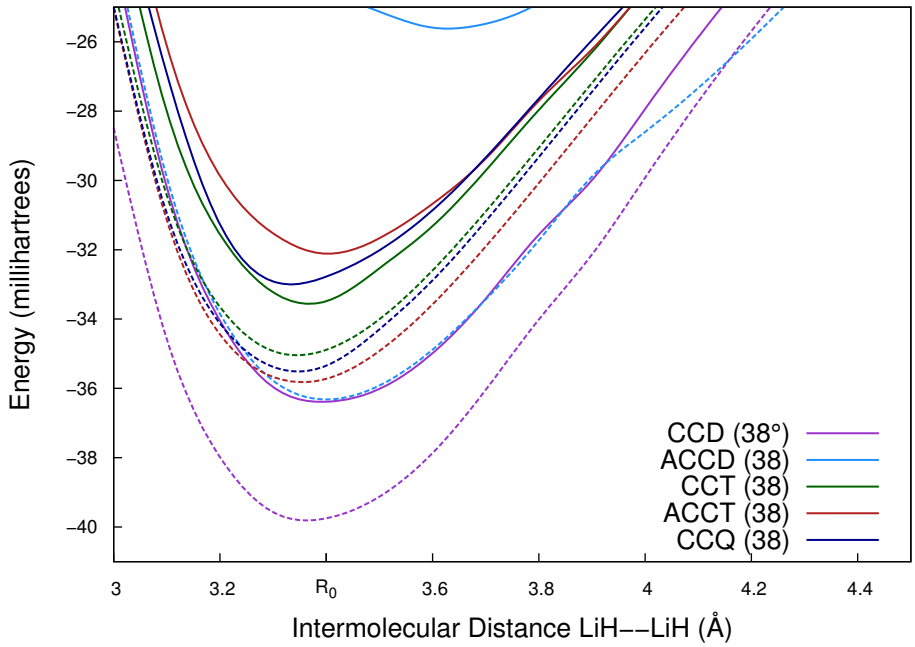

Figure 5.5: The equilibrium regime of 5.4 shown in more detail. Solid lines have been counterpoise corrected and broken lines are the uncorrected interaction energies.

Figs. 5.2 and 5.3 demonstrates that our monomer re-optimization and subsequent basis set truncation is capable of obtaining lower, more stable energies, but with only minor changes in the BE.

5.5.3 Computational Resource Advantages

Because the monomer-optimized basis set routine does not have BSSE, we save a significant amount of computational effort since the CP correction requires a full dimer basis calculation for each monomer. Essentially three calculations with the same number of orbitals must be executed due to the ghost atoms, an expensive prospect when using large basis sets or if a greater number of monomers is desired for a trimer or larger cluster.

With our method, two monomer trials are all that is necessary to generate the dimer (or one if the dimer is a homodimer). Due to the exponential scaling of the ACSE method and most other high accuracy electronic structure routines, single monomer calculations

with their lesser number of orbitals is highly desirable over a dimer calculation. Table 5.5 displays the average times for the monomer ACSE calculations to converge. Assuming that

Table 5.5: The average ACSE calculation time for a single monomer using one CPU. Time is measured in seconds (s) or minutes (m). *Note:* Only one trial was computed for the CCQ monomer.

	CCD	ACCD	CCT	ACCT	CCQ
Avg time	6.0(s)	62.6 (s)	2.49 (m)	48.79 (m)	202.85 (m)

the system involves monomers of several different species, each monomer could be computed separately as well.

When it comes to the dimer ACSE calculations however, the truncation aspect of our optimization procedure reduces the computational expense by literal orders of magnitude. Whereas the ACSE dimer calculation with a full CCQ basis of 170 MOs may take between

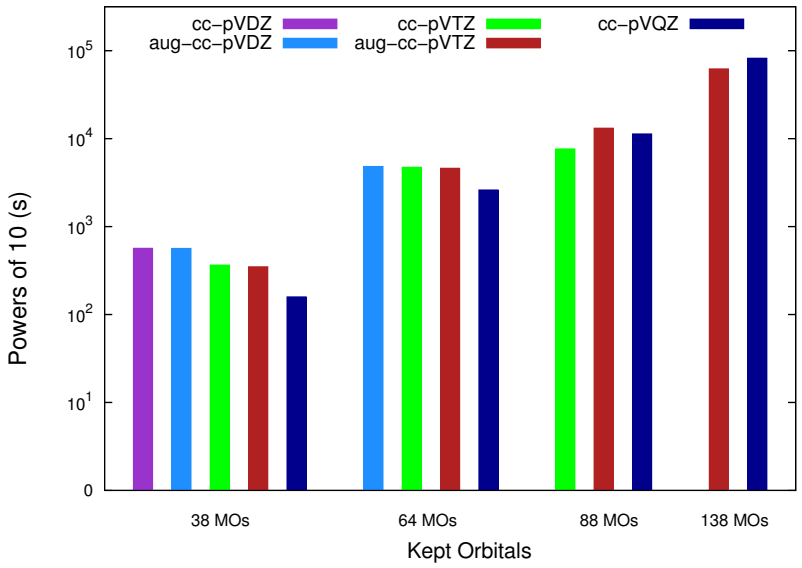

Figure 5.6: Average times for dimer ACSE calculations for each basis set size with a logarithmic scale for time measured in seconds.

50 and 80 hours to converge with a single CPU, we can compute a better, more stable energy with the same BE without the need for a CP correction in several minutes by using monomer-optimization and truncation. See Fig. 5.6 for numerical details.

5.6 Conclusion

We have shown that the monomer-optimized basis set approach can provide extremely accurate energetic predictions for dimers by using large AO basis sets to express an ideal subset of MOs uniquely selected by the monomer itself. This process captures the BE of the $(LiH)_2$ linear dimer for geometries both near and distant from the computed equilibrium configuration. Moreover, because we build the dimer from individually computed monomers we do not have the artificial energy stabilization caused by BSSE and thus no CP correction is required. The removal of excess orbital permits us to reap all of these benefits, but at a fraction of the computational cost.

This procedure could be executed with other electronic structure algorithms provided that there is a systematic way to identify the best MOs in the system and then remove them. We chose the 2-RDM ACSE approach because it can correlate the electrons in all orbitals, not just those in an active space. This means that we can investigate systems that require single- or multi-referenced treatment, including those whose degree of correlation changes with geometry or excitation level. The ACSE routine also provides us with an expedient and straightforward way to compute the best MOs for a given system in a basis by contracting the 2-RDM and diagonalizing the resultant 1-RDM to obtain the NOs. This coupled with associated NO occupation numbers makes the orbital optimization and truncation a simple process.

Future work will examine other systems, both larger and more strongly correlated and perhaps small trimers. We also intend to investigate how well this system predicts energies in the van der Waals regions by fitting the Leonard-Jones potential equation to our results. The monomer-optimized basis set routine used with the ACSE algorithm represents a new effective and inexpensive way to investigate intermolecular interactions.

5.7 References

[1] M. W. Schmidt and M. S. Gordon, "The construction and interpretation of MCSCF wavefunctions.," *Annu. Rev. Phys. Chem.*, vol. 49, pp. 233–66, jan 1998.

[2] A. I. Krylov, "Equation-of-motion coupled-cluster methods for open-shell and electronically excited species: the Hitchhiker's guide to Fock space.," *Annu. Rev. Phys. Chem.*, vol. 59, pp. 433–62, jan 2008.

[3] P. W. Atkins and J. de Paula, *Atkins' Physical Chemistry*. New York: Oxford University Press, 8 ed., 2006.

[4] N. S. Szabo, Attila; Ostlund, *Modern Quantum Chemistry: Introduction to Advanced Electronic Structure Theory*. Mineola, New York: Dover Publications, Inc., 1 ed., 1982.

[5] M. S. Gordon, D. G. Fedorov, S. R. Pruitt, and L. V. Slipchenko, "Fragmentation Methods: A Route to Accurate Calculations on Large Systems," *Chem. Rev.*, vol. 112, pp. 632–672, jan 2012.

[6] G. Gidofalvi and D. A. Mazziotti, "Molecule-optimized basis sets and Hamiltonians for accelerated electronic structure calculations of atoms and molecules.," *J. Phys. Chem. A*, vol. 118, pp. 495–502, jan 2014.

[7] D. A. Mazziotti, "Anti-Hermitian Contracted Schrödinger Equation: Direct Determination of the Two-Electron Reduced Density Matrices of Many-Electron Molecules," *Phys. Rev. Lett.*, vol. 97, p. 143002, oct 2006.

[8] G. Gidofalvi and D. A. Mazziotti, "Molecular properties from variational reduced-density-matrix theory with three-particle N-representability conditions.," *J. Chem. Phys.*, vol. 126, p. 024105, jan 2007.

[9] E. J. Sturm and D. A. Mazziotti, "Highly accurate excited-state energies from direct

computation of the 2-electron reduced density matrix by the anti-Hermitian contracted Schrödinger equation," *Mol. Phys.*, vol. 114, pp. 335–343, sep 2015.

[10] F. Jensen, *Introduction to Computational Chemistry, 2nd Edition.* West Sussex, England: Wiley, 2nd ed., 2007.

[11] D. A. Mazziotti, "Anti-Hermitian part of the contracted Schrödinger equation for the direct calculation of two-electron reduced density matrices," *Phys. Rev. A*, vol. 75, p. 022505, feb 2007.

[12] D. A. Mazziotti, "Two-electron reduced density matrices from the anti-Hermitian contracted Schrodinger equation: enhanced energies and properties with larger basis sets.," *J. Chem. Phys.*, vol. 126, p. 184101, may 2007.

[13] P.-O. Löwdin and H. Shull, "Natural Orbitals in the Quantum Theory of Two-Electron Systems," *Phys. Rev.*, vol. 101, pp. 1730–1739, mar 1956.

[14] B. O. Roos, "Complete active space (CAS) SCF study of the dipole polarizability function for the X 1Σ+ state of LiH," *J. Chem. Phys.*, vol. 76, no. 11, p. 5444, 1982.

[15] S. A. C. McDowell, "A computational study of the LiH dimer," *J. Comput. Chem.*, vol. 24, pp. 1201–1207, jul 2003.

[16] Y.-L. Chen, C.-H. Huang, and W.-P. Hu, "Theoretical Study on the Small Clusters of LiH, NaH, BeH 2 , and MgH 2," *J. Phys. Chem. A*, vol. 109, pp. 9627–9636, oct 2005.

[17] X. Wang and L. Andrews, "The activation of hydrogen by Li atoms to form [(LiH)2]," *Angew. Chemie - Int. Ed.*, vol. 46, pp. 2602–2606, apr 2007.

[18] NIST, "Computational Chemistry Comparison and Benchmark DataBase," 2015.

[19] D. Feller, "The role of databases in support of computational chemistry calculations," *J. Comput. Chem.*, vol. 17, pp. 1571–1586, oct 1996.

[20] K. L. Schuchardt, B. T. Didier, T. Elsethagen, L. Sun, V. Gurumoorthi, J. Chase, J. Li, and T. L. Windus, "Basis set exchange: A community database for computational sciences," *J. Chem. Inf. Model.*, vol. 47, pp. 1045–1052, may 2007.

[21] M. W. Schmidt, K. K. Baldridge, J. A. Boatz, S. T. Elbert, M. S. Gordon, J. H. Jensen, S. Koseki, N. Matsunaga, K. A. Nguyen, S. Su, T. L. Windus, M. Dupuis, and J. A. Montgomery, "General atomic and molecular electronic structure system," *J. Comput. Chem.*, vol. 14, pp. 1347–1363, nov 1993.

[22] A. Kaczmarek, A. J. Sadlej, and J. Leszczynski, "First-order interaction energies and the basis set truncation effects," *Mol. Phys.*, vol. 104, pp. 395–407, feb 2006.

[23] S. Boys and F. Bernardi, "The calculation of small molecular interactions by the differences of separate total energies. Some procedures with reduced errors," *Mol. Phys.*, vol. 19, pp. 553–566, oct 1970.

[24] P. Valiron and I. Mayer, "Hierarchy of counterpoise corrections for N-body clusters: generalization of the Boys-Bernardi scheme," *Chem. Phys. Lett.*, vol. 275, pp. 46–55, aug 1997.